

CHARACTERIZATION OF HALOGEN-BONDED COMPLEXES IN
SYSTEMS WITH COMPETING HYDROGEN BONDING OR
ELECTRON TRANSFER

A THESIS

SUBMITTED TO THE GRADUATE SCHOOL
IN PARTIAL FULFILLMENT OF THE REQUIREMENTS

FOR THE DEGREE

MASTERS OF SCIENCE

BY

EMMANUEL ADENIYI

DR. SERGIY ROSOKHA - ADVISOR

BALL STATE UNIVERSITY

MUNCIE INDIANA

JULY 2023

ABSTRACT

THESIS: Characterization of Halogen Bonded Complexes in Systems with Competing Hydrogen Bonding or Electron Transfer

STUDENT: Emmanuel Adeniyi

DEGREE: Master of Science

COLLEGE: Science and Humanities

DATE: July 2023

PAGES: 91

Halogen bonding (HaB) is an intermolecular attraction between covalently bonded electron-poor halogen atoms and electron-rich species, similar to hydrogen bonding (HyB). The strengths of HaB and HyB are similar, and if a molecule contains both halogen and hydrogen substituents, these bonds may compete or cooperate. To understand the behavior of such molecules, it is necessary to identify these bonds. In this study, HaB and HyB coexisting in solution were differentiated, and the mode of interaction of these molecules was determined using a combination of UV-Vis and NMR spectroscopy, and computational analysis. These studies showed that HaB complexes of haloforms with aromatic and aliphatic amines exhibit strong absorption bands in their UV-Vis spectra. In comparison, the spectra of the HyB complexes were a superposition of the spectra of their individual reactants. The effects of bonding on NMR spectra depend on the nature of the amine. HyB and HaB with aliphatic amines led to a shift in the proton signals of the NMR spectrum in opposite directions. Studies of HaB and HyB complexes in a solution of (halo)imidazolium and halides have confirmed these distinctions. Overall, this study showed that

combining UV-Vis and NMR measurements allowed us to distinguish between the formation of competing HaB and HyB complexes in the solution. In addition to the formation of the HaB complex, a redox reaction can occur when all electrons are transferred from the electron donor (HaB acceptor) to the electron acceptor (HaB donor). To evaluate the role of the HaB complexes in these processes, we studied the interactions between molecular iodine and various anilines or heterocyclic compounds. This study indicates that HaB complexes represent intermediates of electron transfer reactions and that HaB can significantly reduce the activation barriers for electron transfer.

ACKNOWLEDGEMENTS

I am grateful for God's grace, which enabled me to complete my Master's program. I would like to take this opportunity to express my appreciation to those who have contributed significantly to my academic journey.

I am immensely grateful to Dr. Sergiy Rosokha, my research advisor, for his invaluable guidance and mentorship throughout my research project. I would also like to extend my heartfelt thanks to Brandon Watson, Olivia Grounds, and Lauryn Snowden from Dr. Rosokha's group for their assistance in collecting preliminary spectral and computational data for this study. Additionally, I am thankful to Dr. Matthias Zeller for conducting the X-ray crystallographic measurements of several complexes.

I am equally appreciative of the members of my research committee, Dr. Emil Khisamutdinov and Dr. Jesse Tye, for their willingness to participate in this research project. I am grateful to the Chemistry Department at Ball State University for providing me with the opportunity to pursue my studies. Furthermore, I would like to express my special gratitude to the National Science Foundation (grant number CHE2003603) for their financial support, which has been invaluable in enabling me to achieve my academic goals. I would also like to take this opportunity to thank my family and friends for their assistance and support.

TABLE OF CONTENTS

ABSTRACT.....	i
ACKNOWLEDGEMENTS.....	iii
TABLE OF CONTENTS.....	iv
LIST OF TABLES.....	xi
STRUCTURES AND ABBREVIATIONS.....	xiii
CHAPTER 1.....	1
INTRODUCTION AND LITERATURE REVIEW.....	1
1.1 Hydrogen Bonding (HyB).....	1
1.2 Halogen Bonding (HaB).....	3
1.2.1 Electrostatic (σ -Hole) Model of Halogen Bonding.....	5
1.2.2 Applications of Halogen Bond.....	7
1.3 Computational Investigations of Halogen and Hydrogen Bonding.....	11
1.4 HyB/HaB Complementarity and Competition in Solid State.....	13
1.5 Previous Studies on Halogen and Hydrogen Bonding in Solution.....	15
1.6 Electron Transfer Reaction.....	18
1.7 Halogen Bond and Electron Transfer Reaction.....	22
CHAPTER 2.....	25
EXPERIMENTAL SECTION.....	25
2.1 Materials.....	25
2.2 X-ray Crystallography Analysis.....	25

2.3	UV-Vis Spectroscopic Measurements	27
2.4	¹ H NMR Spectroscopic Measurements.....	28
2.5	Gaussian Computations.....	29
2.6	Calculation of K and ε Values of the HaB and HyB Complexes.....	30
RESULTS AND DISCUSSION.....		33
CHAPTER 3. HALOGEN- AND HYDROGEN-BONDED COMPLEXES OF HALOFORMS WITH ALIPHATIC AND AROMATIC AMINES.....		33
3.1	X-ray Crystallographic Analysis.....	33
3.2	UV-Vis Measurements of HaB and HyB Complex in Solution.	35
3.3	¹ HNMR Measurement of HaB and HyB Complex in Solution.	38
3.4	Computational Data.....	40
3.5	Simultaneous Treatment of the Experimental UV-Vis and NMR Data.....	52
CHAPTER 4. HALOGEN AND HYDROGEN BONDING BETWEEN (HALO)IMIDAZOLIUM CATIONS AND HALIDES		54
4.1	UV-Vis Measurement of HaB and HyB Complex in Solution.	54
4.2	¹ HNMR Measurement of HaB and HyB Complex in Solution	58
4.3	Computational Data.....	60
CHAPTER 5. ELECTRON TRANSFER REACTION BETWEEN IODINE WITH AMINES AND SOME HETEROCYCLIC COMPOUNDS		63
5.1	X-ray Crystallographic Analysis.....	63

5.2.	UV-Vis Measurement of HaB Complex in Solution.	64
5.3	Computational Data.....	68
5.4	Conclusion.....	71

LIST OF FIGURES

Figure 1-1. Schematic representation of the hydrogen bonding.	1
Figure 1-2. X-ray crystal structures showing hydrogen bonds between (halo)imidazolium and halides (CSD Refcode PAWXES01).	2
Figure 1-3. Schematic representation of halogen bonding.	3
Figure 1-4. X-ray crystal structures showing I··I halogen bond from trimethylamine to iodine (CSD Refcode TMEAMI).	4
Figure 1-5. X-ray crystal structures showing I··I halogen bond from 4,5-dichloro-1,3-bis(2,6-diisopropylphenyl)-2-iodoimidazolium to iodide (CSD Refcode GEPHAN).	5
Figure 1-6. Molecular electrostatic potential, in Hartree's, at the 0.001 e/bohr ³ isodensity surface of CF ₃ X (from left to right, X = Cl, Br, I).	6
Figure 1-7: Halogen bond in crystal engineering showing the projection view, along the stacking axis, of the unit cell of the salt ties of (38) ₄ •(1,5-Napht(SO ₃) ₂) = 1,5-naphthalenebis-(sulfonate), showing the HaBs as dotted lines.	8
Figure 1-8. Halogen Bond in biochemical systems showing Holiday junctions in the DNA structure.	9
Figure 1-9. Halogen bond in medicinal chemistry and chemical biology.	10
Figure 1-10. Halogen bonding in the catalytic polymerization of l-lactide to poly(l-lactide) with ICl ₃	10
Figure 1-11. Structures of TEMPO•••CHX ₃ optimized by wB97XD/aug-cc-pVDZ(-PP).	13
Figure 1-12. Crystal structures showing I··S halogen bonds between iodotetrafluorobenzoic acid and dithiane (CSD Refcode HIZQOY).	14

Figure 1-13. Crystal structure of benzyltrimethylammonium iodide iodoform solvate showing halogen and hydrogen bonds between CHI_3 and I^- as blue lines.	14
Figure 1-14. X-ray crystal structure of the complex between hexamethylphosphoramide and halothane with hydrogen and halogen bonds.....	15
Figure 1-15. Halogen and hydrogen bonding of haloforms complexes with halides in solution. ³³	16
Figure 1-16. UV-Vis spectra of the solutions with a constant concentration of iodoform compound and varied concentration of iodide.....	17
Figure 1-17. Dependencies of proton NMR shifts of CHX_3 (in CD_3CN , 22°C , relative to those in the separate molecules) on the concentration of added Pr4NA salts.	18
Figure 1-18. Illustration of outer-sphere and inner-sphere reaction	20
Figure 1-19. Illustration of energy diagram of Marcus Theory	20
Figure 1-20. Inner sphere electron transfer via a halogen-bonded complex between tribromonitromethane and iodide anion. ⁴⁰	23
Figure 3-1. X-ray structures of iodoform co-crystals with TMPD (A:1:1, B:2:1) and DABCO (C) showing alternating halogen (and hydrogen) bonded zigzag chains represented with the blue lines.	34
Figure 3-2. UV-Vis spectra of solutions with constant concentrations of CHI_3 (0.01M) and various concentrations of 1,4-diazabicyclo[2,2,2]octane (DABCO).....	36
Figure 3-3. UV-Vis spectra of solutions with a constant concentration of CHBr_3 (0.01M) and various concentrations of DABCO..	37
Figure 3-4. UV-Vis spectra of solutions with constant concentrations of CHI_3 (0.01M) and various concentrations of tetramethyl-p-phenylenediamine (TMPD)..	38

Figure 3-5. ^1H NMR shifts occurring upon the addition of DABCO to solutions containing CHI_3 (A), CHBr_3 (B), and CHCl_3 (C).....	39
Figure 3-6. ^1H NMR shifts occurring upon addition of TMPD to solutions containing CHI_3 (A), CHBr_3 (B), and CHCl_3 (C).....	40
Figure 3-7. Electrostatic potential (calculated at 0.001 electrons Bohr ⁻³ electronic density) on the molecular surfaces of CHI_3 , CHBr_3 , CHCl_3 , DABCO, and TMPD.	46
Figure 3-8. Correlations between the interaction energies in the HaB and HyB complexes with DABCO and TMPD.....	48
Figure 3-9. Superposition of the results of the QTAIM and NCI analyses on the structures of the HaB complexes of CHBr_3 with DABCO (A) and TMPD (C) and HyB complexes with DABCO (B) and TMPD (D).....	49
Figure 3-10. Effect of variations in interatomic H...N and X...N separations on the energies of HyB and HaB complexes.....	50
Figure 3-11. Structural overlap of the associations between TMPD and CHI_3 (left), CHBr_3 (middle), and CHCl_3 (right) formed via H...N bonding and alternative complexes (shown as red structures).....	51
Figure 3-12. Dependencies of ΔAbs and $\Delta\delta$ values in solutions with constant concentration of CHI_3 (0.01 M) and variable concentrations of DABCO.....	52
Figure 4-1. UV-Vis spectra of solutions with constant concentrations of H-Im-iPrArI (0.4mM) and various concentrations of tetrabutylammonium iodide (TBAI).....	55
Figure 4-2. Dependencies of Abs values in solutions with constant concentrations of H-Im-iPrArI (0.4mM) and variable TBAI concentrations. The solid lines show the fitting of the UV-Vis titration data.....	55

Figure 4-3. UV-Vis spectra of solutions with constant concentrations of H-Im-iPrArI (0.4mM) and various concentrations of tetrabutylammonium bromide (TBABr).....	56
Figure 4-4. Dependencies of the Δ Abs values in the solutions with a constant concentration of H-Im-iPrArI (0.4mM) and variable TBABr concentrations.....	56
Figure 4-5. UV-Vis spectra of solutions with constant concentrations of H-Im-iPrArH (0.4mM) and various concentrations of tetrabutylammonium iodide (TBAI).....	57
Figure 4-6. The dependencies of the δ values in solutions with a constant concentration of H-Im-iPrArH and variable concentrations of TBACl, TBABr, and TBAI.....	58
Figure 4-7. The dependencies of the δ values in solutions with a constant concentration of H-Im-iPrArI and variable concentrations of TBACl, TBABr, and TBAI.	59
Figure 4-8. Molecular orbital interaction diagrams	61
Figure 5-1. X-ray structures showing the formation of redox products from the interaction of I ₂ and MPTZ (left), I ₂ , and pMeODMA (right).....	64
Figure 5-2. UV-Vis spectra of solutions with constant concentrations of I ₂ and various concentrations of DMABr in DCM.	65
Figure 5-3. UV-Vis spectra of solutions with constant I ₂ concentrations and various PTZ concentrations in DCM.	66
Figure 5-4. Dependencies of the Δ Abs and $\Delta\delta$ values in the solutions with a constant concentration of I ₂ and variable aliphatic and aromatic amine concentrations.	68

LIST OF TABLES

Table 2-1. Crystallography, data collection, and refinement details.....	27
Table 2-2: Example of the volumes used for each trial in mL for a typical UV-Vis experiment	28
Table 2-3: Example of volumes used for each trial in mL for a typical ¹ HNMR experiment.	29
Table 3-1. Energies of HaB and HyB complexes between haloforms and amines resulting from M06-2X/def-TZVPP computations	41
Table 3-2: Optimized structures of the calculated complexes with amines, where HaB shows a linear bond angle and HyB shows a deviation from the linear bond angle.	42
Table 3-3: Interatomic distances and angles in the HaB and HyB complexes	43
Table 3-4: Calculated UV-Vis and NMR characteristics of the HaB and HyB complexes.....	45
Table 3-5. V _{max} values on the surfaces of halogen (V ^X) and hydrogen (V ^H) atoms (at 0.001 a.u. electron density) in the individual haloforms and the molecules polarized by the presence of electron-rich centers near halogen (in the HaB complex) or hydrogen (in the HyB complex) atoms.	47
Table 3-6. Electron densities and energies (ρ(r) and H(r), in a.u.) at BCPs along HaB and HyB bond paths.	49
Table 3-7. Formation constants of HaB and HyB Complexes of CHI ₃ and CHBr ₃ with DABCO and TMPD complexes.....	53
Table 4-1: Formation constants, wavelengths and the coefficients of absorptivity of halogen-bonded complexes.....	57
Table 4-2. The K values obtained by the nonlinear fitting algorithm of the NMR data in OriginPro (2016).....	59

Table 4-3: Energies and UV-Vis values of HyB and HaB complexes between (halo)imidazolium and halides, and NBO charges on the halides, obtained from M06-2X/def-TZVPP computations (acetonitrile)..... 60

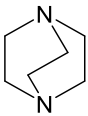
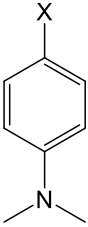
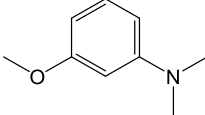
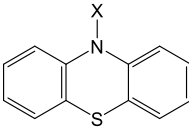
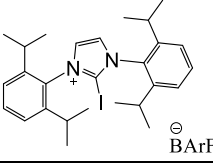
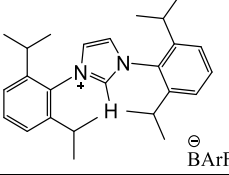
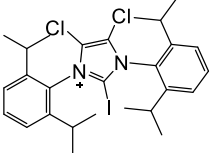
Table 4-4 Contribution of different components to interaction energies between imidazolium cations and halides (from EDA) and charge transfer (Δq) in the corresponding complexes values between (halo)imidazolium and halides 62

Table 5-1. Formation constants and coefficients of absorptivity of halogen bonded complexes 67

Table 5-2: Energies of HaB complexes between I₂ and amines obtained from M06-2X/def-TZVPP computations (in vacuum, dichloromethane, and acetonitrile) using PCM model..... 68

Table 5-3: Energies ET reactions of HaB complexes between I₂ and amines resulting from M06-2X/def-TZVPP computations (vacuum, dichloromethane, and acetonitrile) using the PCM model. 70

STRUCTURES AND ABBREVIATIONS

Abbreviations	Definition	Structures
DABCO	1, 4-diazabicyclo[2.2.2]octane	
a. DMAF b. DMABr c. pMeODMA d. DMACN e. TMPD	X a. F: 4-Fluoro-N,N-dimethylaniline b. Br: 4- Bromo-N,N-dimethylaniline c. OCH ₃ : 4-Methoxy-N,N-dimethylaniline d. CN: 4-cyano-N, N-dimethylaniline e. N(CH ₃) ₃ : N,N,N',N'-tetramethyl-p-phenylenediammine	
mMeODMA	3-Methoxy-N,N-dimethylaniline	
a. PTZ b. MPTZ	Heterocyclic compounds (X=H, CH ₃) a. Phenothiazine b. 10-methylphenothiazine	
H-Im-iPrAr-I/BArF	N,N'-1,3-Bis(2,6-diisopropylphenyl)-2-iodoimidazolium tetrakis[3,5-bis(trifluoromethyl)phenyl]-borate	
H-Im-iPrAr-H/BArF	N,N'-1,3-Bis(2,6-diisopropylphenyl)-imidazolium tetrakis[3,5-bis(trifluoromethyl)phenyl]-borate	
Cl-Im-iPrAr-I/OTf	4,5-dichloro-1,3-bis(2,6-diisopropylphenyl)-2-iodoimidazolium triflate	
TEA	Triethylamine	
AN	Acetonitrile	
DCM	Dichloromethane	
PCM	Polarizable continuum model	
TD	Time-dependent	
NBO	Natural bond orbital	
EDA	Energy decomposition analysis	
QTAIM	Quantum theory of atom in molecule	
TBAX	Tetrabutylammonium halide	

CHAPTER 1

INTRODUCTION AND LITERATURE REVIEW

1.1 Hydrogen Bonding (HyB)

Hydrogen bonding is an intermolecular interaction that plays a crucial role in various chemical and biological processes. An early definition of hydrogen bonding is that of Pimentel and McClellan, who wrote that a hydrogen bond exists if there is evidence of bonding that involves hydrogen already bonded to another atom and another electronegative atom.¹ In a hydrogen bond complex (R-H•••Y), group R-H is referred to as the HyB donor and Y is the HyB acceptor.² A schematic representation of the hydrogen bond is shown in Figure 1-1 (Where R = C, halogen, nitrogen, etc., Y= N, O, S, Se or I, Cl⁻, Br⁻, F⁻; X-H = HyB donor; Y = HyB acceptor; R-H •••Y = HyB complex; and ••• = indicates attractive noncovalent interactions).



Figure 1-1. Schematic representation of the hydrogen bonding.

Hydrogen bonding is a relatively strong type of intermolecular attraction, which can significantly affect the physical and chemical properties of a substance. For example, hydrogen bonding is responsible for the high boiling point and surface tension of water as well as the unusual density behavior of ice compared to other solids. In addition to its important physical and chemical properties, hydrogen bonding also plays a crucial role in biological systems. For instance, it helps stabilize the secondary and tertiary structures of proteins and nucleic acids, and is involved in the recognition and binding of biomolecules such as enzymes, antibodies, and hormones. Strong hydrogen bonds may resemble covalent bonds in most properties, and weak HyB can hardly be distinguished from van der Waals interactions. There are continuous transitions to effects that are

as diverse as covalent bonds and pure ionic, cationic, and van der Waals interactions. The H---Y distance was shorter than the sum of the van der Waals radii for most hydrogen bonds. For an R-H group to form hydrogen bonds, R does not need to be highly electronegative, and it is only necessary that R-H is at least slightly polar. The energy range for hydrogen bond dissociation spans more than two powers of ten, about 0.2 to 40 kcalmol⁻¹, and the possible functions of a particular type of hydrogen bond depend on its position on this scale.²

An example of HyB relevant to this work was studied when the imidazolium cation interacts with halides and the hydrogen atom forms hydrogen bonds with the negatively charged halide atom, such as chlorine, bromine, or iodine. Figure 1-2 below illustrates the X-ray crystal structures displaying HyB interaction between imidazolium cations and halides.

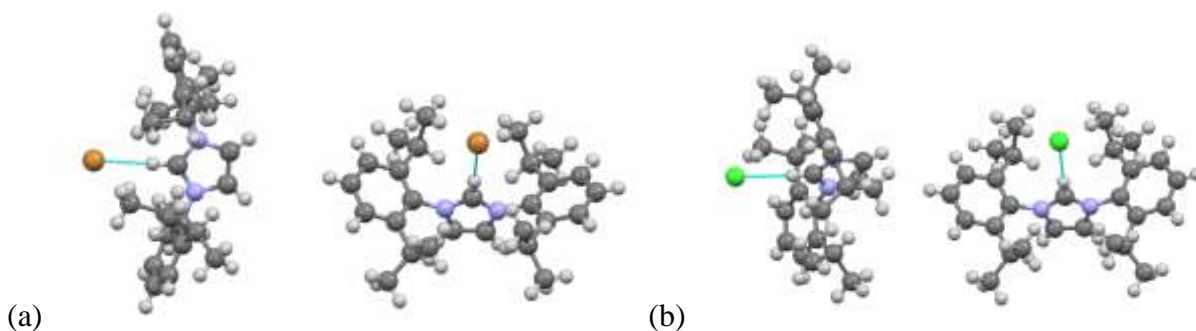


Figure 1-2. X-ray crystal structures showing (a) H···Br hydrogen bond from N,N'-1,3-Bis(2,6-diisopropylphenyl)-2-iodoimidazolium to bromide (CSD Refcode OBASET), (b) H···Cl hydrogen bond from N,N'-1,3-Bis(2,6-diisopropylphenyl)-2-iodoimidazolium to chloride (CSD Refcode PAWXES01).³

The distance between the hydrogen atom in the imidazolium cation and the negatively charged halide atom gives an idea about the strength of the hydrogen-bonding interaction. The bond distances between the hydrogen atom in the imidazolium cation and the negatively charged halide atom were H---Br (2.438 Å) and H---Cl (2.499 Å). While the sum of the van der Waals radii of the respective H---X are 3.05 Å (H---Br), and 2.95 Å (H---Cl), respectively. From the given bond

distances and van der Waals radii, it was observed that the HyB distance is shorter than the sum of the Van der Waals radii in all cases, indicating a significant hydrogen-bonding interaction between the imidazolium cation and halides. The shorter the bond distance, the stronger the hydrogen bonding interaction, as seen in the H---Br bond.^{3,4}

1.2 Halogen Bonding (HaB)

Halogen bonds are similar to hydrogen bonds and, in recent years, have played an essential role in supramolecular systems. According to the IUPAC definition, "A halogen bond occurs when there is evidence of a net attractive interaction between an electrophilic region associated with a halogen atom in a molecular entity and a nucleophilic region in another, or the same molecular entity."⁵ A schematic representation of the halogen bond is shown in Figure 1-3 below (Where R = C, halogen, nitrogen, etc. X = I, Cl, and Br; Y= N, O, S, Se, I-, Cl-, Br-, F- R-X = halogen bond donor; Y = halogen bond acceptor; R-X...Y = halogen bond complex; and ... = indicates attractive noncovalent interactions).



Figure 1-3. Schematic representation of halogen bonding.

The origin of the HaB story can be dated to approximately two centuries ago when J. J. Colin synthesized $\text{I}_2 \cdots \text{NH}_3$, believed to be the first halogen-bonded complex ever made by a happy accident. Shortly after the discovery of Colin in 1819, P. Pelletier and J. B. Caventou presented the first experimental proof of the possibility of halogens attractively interacting with anions. Specifically, they reported the synthesis of strychnine triiodide, in which the I_3^- anion was formed by the interaction of I^- with I_2 . Several other investigators also cited the triiodide anion formation to explain the increased solubility of I_2 in different solvents upon the addition of metal iodides, as

well as the reaction between metal halides and I₂.⁵ In 1959, Knut Stromme also synthesized a HaB complex by interacting trimethylamine with molecular iodine, (CH₃)₃N•••I₂. Figure 1-4 shows the crystal structure determined from the study.⁶

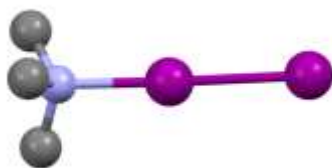


Figure 1-4. X-ray crystal structures showing I•••I halogen bond from trimethylamine to iodine (CSD Refcode TMEAMI).⁶

An interesting characteristic of HaB is that the distance between the interacting nuclei, such as the halogen substituent and nucleophilic site, is less than the sum of their Van der Waals (vdW) radii. In addition, the HaB interaction is usually collinear with the R-X covalent bond, and the angle between the moieties is usually at about 175° (although there are variations due to secondary interactions or crystal packing effects). HaB is analogous in strength (energies up to 200 kJmol⁻¹) to more prominent intermolecular interactions, such as HyB. Similar energetic and geometric feature trends were observed for the HyB and HaB interactions. In addition, the strength of the halogen bonds can be fine-tuned by changing the halogen atom and the moiety to which it is covalently bonded; increasing the electron-withdrawing ability of the substituent results in an increased halogen bond donor strength.

However, while the study of HaB in the solid state has been focused on organic molecules in the past, studies with metal-containing species and anions have gained prominence more recently.⁷⁻⁹ Concerning the interaction between halogens and Lewis bases, stronger halogen bonds are generally observed for nitrogen-containing compounds, such as amine and pyridine derivatives,

than for oxygen- and sulfur-containing compounds, such as ethers, alcohols, and thioethers. Interestingly, N-oxides was preferred over pyridine compounds. In addition, anionic species tend to be better halogen bond acceptors than neutral molecules, allowing HaB to have practical applications in anion coordination chemistry.

An example of halogen bonding relevant to this work is observed between a (halo)imidazolium cation and iodide, which involves a short bond distance of 3.159 Å, shorter than the sum of the van der Waals radii of the two atoms (3.96 Å). This interaction is attractive and involves the iodide ion and iodine atom attached to the nitrogen atom of the haloimidazole ring. Figure 1-5 below depicts halogen bonding between the (halo)imidazolium cation and iodide.

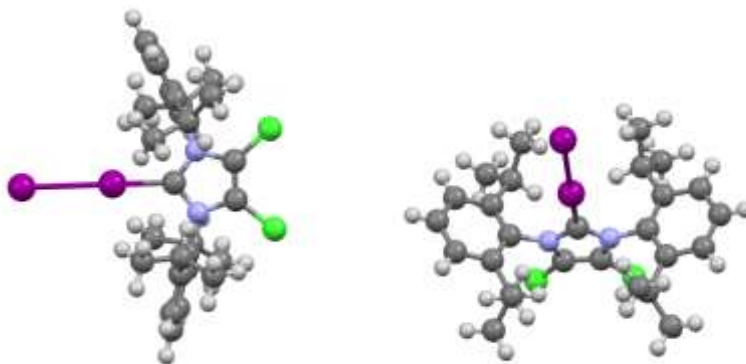


Figure 1-5. X-ray crystal structures showing I \cdots I halogen bond from 4,5-dichloro-1,3-bis(2,6-diisopropylphenyl)-2-iodoimidazolium to iodide (CSD Refcode GEPHAN).¹⁰

1.2.1 Electrostatic (σ -Hole) Model of Halogen Bonding

The exact nature of the halogen bond interaction remains disputed because various factors as electrostatic effects, charge transfer, polarization, and dispersion forces contributed to the nature of the interactions and often depend on the individual interacting species.¹¹ The electron density surrounding the halogens is not uniform. This electron density distribution is anisotropic, resulting in two regions of the electron density. The electropositive region that directly participates in

halogen bonding is located at the tip of the halogen, which points away from the covalent bond. This region is referred to as the sigma-hole (σ -hole). The HaB interaction is highly directional because the σ -hole is located on the elongation of the covalent bond involving the halogen atom, resulting in a depleted electron-density region. It is important to note that short and strong HaBs are more directional than long and weak ones, and reducing the polarizability of the HaB donor slightly decreases linearity.^{12, 13} The potentials for covalently bonded halogen atoms in CF_3X are shown in Figure 1-6.

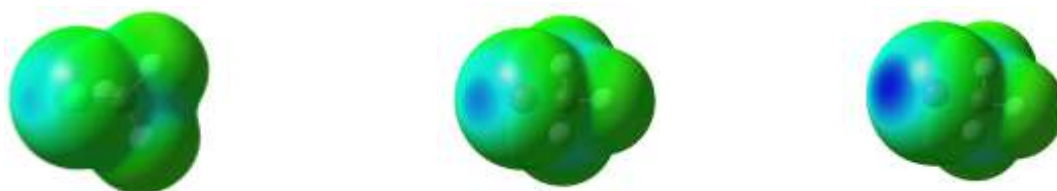


Figure 1-6. Molecular electrostatic potential, in Hartree's, at the 0.001 e/bohr³ isodensity surface of CF_3X (from left to right, X = Cl, Br, I).¹⁴

The electrostatic model explain that it is when atoms are bonded that the surrounding electronic charge is redistributed and then polarized in the direction of the bonding region, which results in regions with greater or lesser electron density at the low or bonding end of the atom.¹⁵

This model efficiently explains the interaction pattern of covalently bonded halogen atoms and their directional preferences, that is, linear interactions with nucleophiles and lateral interactions with electrophiles. The existence of a positive σ -hole accounts for the electrophilic nature of the halogen atoms, while the focused character of the σ -hole explains the high directional dependence of the HaB, and the magnitude of the σ -hole can be correlated with the HaB strength.¹⁶

The significance of σ -hole is associated with the polarizability of the halogen atom. In addition, it dictates the strength of the halogen bond donor in the order $\text{I} > \text{Br} > \text{Cl} > \text{F}$. Fine-tuning of the HaB interaction is possible by modifying the nature of the atom or radical covalently bonded to

the halogen atom in question; an increase in the electron-withdrawing ability of the substituent results in an increased strength of the halogen bond donor. The strength of HaB is directly influenced by the charge transfer occurring between the HaB donor and acceptor. Therefore, acceptor selection can modify the extent of charge transfer, and generally, more basic acceptors increase charge transfer.¹⁷

1.2.2 Applications of Halogen Bond

Halogen bonding (HaB) has recently evolved from scientific curiosity to a widely used chemical interaction for directing and controlling assembly phenomena in crystal engineering, which is a well-defined area that focuses on understanding intermolecular interactions to control the assembly of molecular building blocks into designed architectures. Recently, HaB has been employed in numerous functional applications. In the solid phase, these applications encompass liquid crystals preparation, nonlinear optics, modulation of electrical and magnetic properties, isomer separation, and regulation of solid-state reactions. In the solution phase, HaB finds utility in catalysis, interactions with metal complexes, anion binding in both solution and solid states, biological systems, drug design, and protein-ligand complexation.¹⁸ HaB interactions can be used to build robust supramolecular networks with interpenetrated networks. The HaB donor and acceptor units can assemble highly interpenetrated architectures with different topologies and connectivities. HaB-based crystal engineering can control the solid-state organization of radical species, leading to predictable crystal design and control of the conductivity and magnetic interaction pathways.^{19, 20} An application of halogen bonding in crystal engineering for example, the design of halogen-bonded conductive materials is largely based upon the use of halogenated tetrathiafulvalene (TTF) derivatives as HaB donors and organic sulfonates as HaB acceptors. The

crystal packing of the resultant structures was driven by I...O HaBs and this is illustrated in the Figure 1-7 below.^{9, 21}

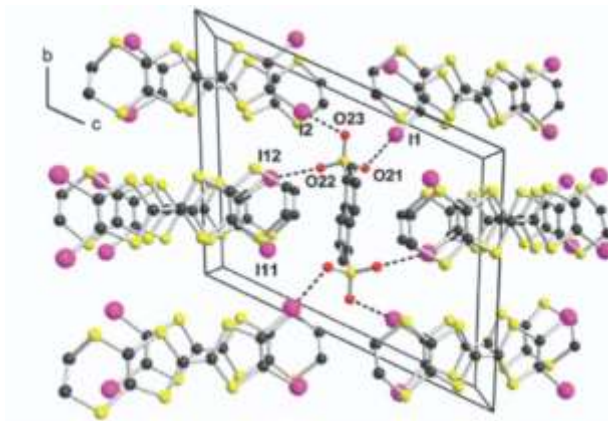


Figure 1-7: Halogen bond in crystal engineering showing the projection view, along the stacking axis, of the unit cell of the salt ties of $(38)_4 \cdot (1,5\text{-Napht}(\text{SO}_3)_2 = 1,5\text{-naphthalenebis-(sulfonate)})$, showing the HaBs as dotted lines.²²

HaB interactions are present in most biological systems, ranging from their ability to hold the nitrogenous bases of DNA together with the binding substrates to the active site of enzymes, and also help to give proteins their secondary structure. In addition, in halogen-bonded Holiday junctions, the unusually short bond between the Br atom of a brominated uracil residue and phosphate oxygens in a four-stranded DNA junction is an example of non-covalent halogen bonding as illustrated in Figure 1-8.²³

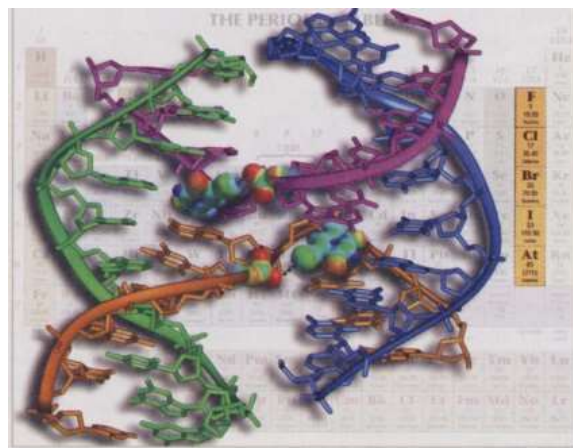


Figure 1-8. Halogen Bond in biochemical systems showing Holiday junctions in the DNA structure.²³

In addition, research has shown that nearly 40% of drugs in testing or on the market in 2014 contained at least one halogen atom. In the same year, it was documented that nearly 20% of cancer-screening drug trials were halogenated. In protein crystallography, researchers study the three-dimensional structures of proteins by analyzing the arrangement of atoms in their crystal lattices. Sometimes, during the analysis, unexpected short contacts between halogen atoms (such as iodine, bromine, or chlorine) and neighboring amino acid residues were observed. These short contacts resulted from halogen bonding interactions. The serendipitous observation of short contacts between halogen atoms and protein structures can provide valuable insights into protein folding, stability, and function. This discovery opens up avenues for understanding protein behavior and designing improved therapeutic agents. HaB has been exploited for molecular recognition and rational drugs design. Figure 1.9 below illustrates the application of halogen bonding in medicinal chemistry and chemical biology.²⁴

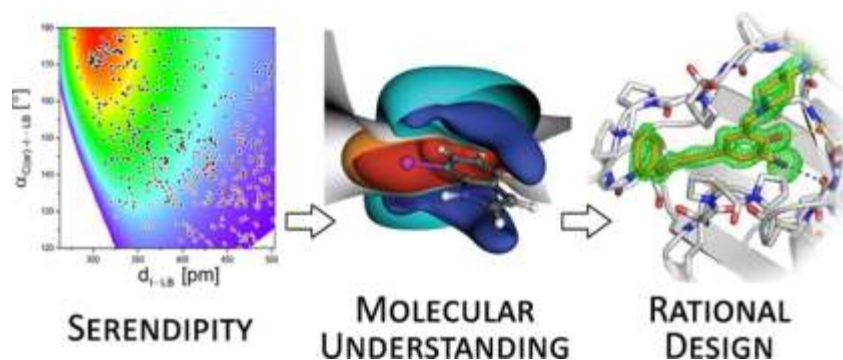


Figure 1-9. Halogen bond in medicinal chemistry and chemical biology.²⁴

Halogen-bonded systems have potential as catalysts in organic synthesis because of their higher directionality and hydrophobicity than hydrogen-bonded systems. Halogen-bonded adducts can act as transient species in different types of reactions, including alkene bromination and metathesis. Elemental iodine and iodine trichlorides have been reported to catalyze organic reactions. ICl_3 electrophilically activates the carbonyl group of L-lactide through the transfer of electron density from oxygen to iodine, while $\text{OH}\cdots\text{Cl}$ hydrogen bonds are formed and HaB and HyB work together to accelerate the reaction in the suggested polymerization pathway. Figure 1-10 shows the application of HaB in organocatalysis.

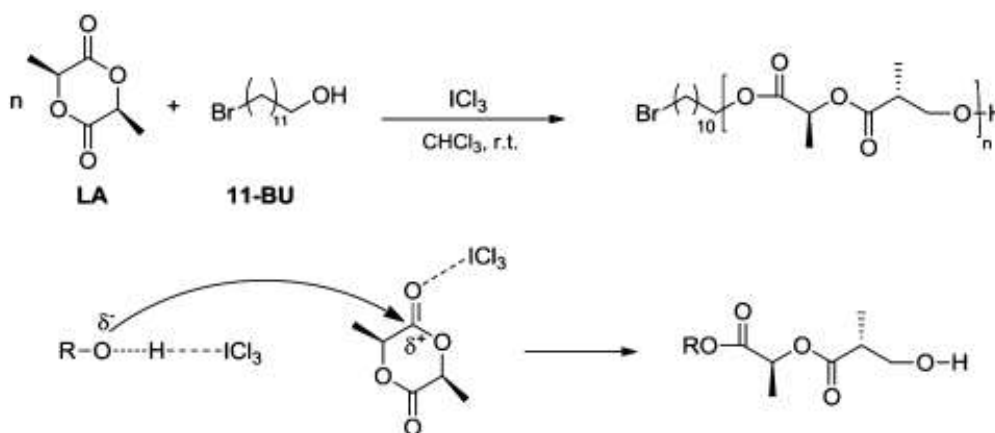


Figure 1-10. Halogen bonding in the catalytic polymerization of l-lactide to poly(l-lactide) with ICl_3 .⁵

1.3 Computational Investigations of Halogen and Hydrogen Bonding

Most of the current knowledge of HaB interactions is based on a combination of quantum mechanical calculations, involving gas-phase investigations, and spectral investigation involving UV/Vis, IR, NMR, and X-ray crystal structure identification; solution-phase examples of HaB interactions are much rarer.¹¹

Quantum mechanics was applied to the investigation of weak intermolecular interactions. More detailed information about molecular geometry, energy, vibrations, and bonding interactions can be unraveled, and there are also uncomplicated approaches that can be employed to investigate the impacts of solvents and neighboring groups computationally.^{22, 25, 26}

HaB interactions are often reasonably weak and their interaction potentials are soft. As a result, only QM calculations at very high levels that consider electron correlation provide reliable results, which in turn are dependent on the selected level of electron correlation. Geometry optimization frequently involves correction of the basis set superposition error (BSSE) using a counterpoise (CP). Density functional theory (DFT) has also been used to describe halogen-bonded complexes. The total interaction energy is partitioned into physically well-known terms using different techniques. Quantum theory of atoms in molecules (QTAIM) and natural bond order analysis (NBO) was also employed to compute the electron density distribution in halogen-bonded complexes and, in some cases, revealed evidence for charge-transfer type interactions.²⁷

Nguyen et al. studied hydrogen-bonded complexes generated by the interaction of trihalomethanes CHX_3 ($\text{X} = \text{F}, \text{Cl}, \text{Br}$) with nitrosyl hydride HNO using ab initio method. The computed binding energies varied from 4 to 8 kJ/mol with ZPE and BSSE corrections. However, while CHBr_3 resulted in the most stable complexes with HNO, CHF_3 formed less-stable associates.

Consequently, the strength of the complexes exhibited an ascending trend from F to Cl to Br. Notably, complex formation led to a reduction in the length of all C-H and N-H bonds, thereby resulting in an increase in their respective stretching frequencies. Thus, a blue shift is found for the N-H bonds of the N-HX type (X = F, Cl, Br).²⁸

Xiao et al. investigated halogen and hydrogen bonding interactions between the 4-hydroxy-2,6,6-tetramethylpiperidine-noxyl radical (TEMPO) an HaB acceptor and trihalomethanes which are HaB and HyB donor, using four different computational methods. The geometric structures of the halogen- and hydrogen-bonded complexes computed using B3LYP, wB97XD, and B97D were similar to the MP2 results. They found that B3LYP method cannot accurately estimate the interaction energies because the dispersion is not considered. In their study, wB97XD and B97D were found to be reasonable alternatives to MP2. The strengths of the halogen and hydrogen bonds followed the order Cl<Br<I. The hydrogen bond interactions were greater than the equivalent halogen bond interactions and should dominate the TEMPO•••CHX₃ system. The halogen bonds became dominant when the halogen atom's most positive value (V_{s, max}) increased. Some of the findings also show that it is likely that halogen bonds predominate in the TEMPO•••CHI₃ complex because of their similar interaction energies and abundant iodine in triiodomethane. Natural bond order (NBO) analysis showed that charge transfer (CT) is essential for forming halogen and hydrogen bonds in this system. As discussed earlier, the nature of halogen and hydrogen bonding is an effect involving multiple interactions, including electrostatic forces (involved in σ -holes), dispersion effect, and charge transfer.²⁹ Figure 1-11 below shows the computational studies of TEMPO with haloforms.

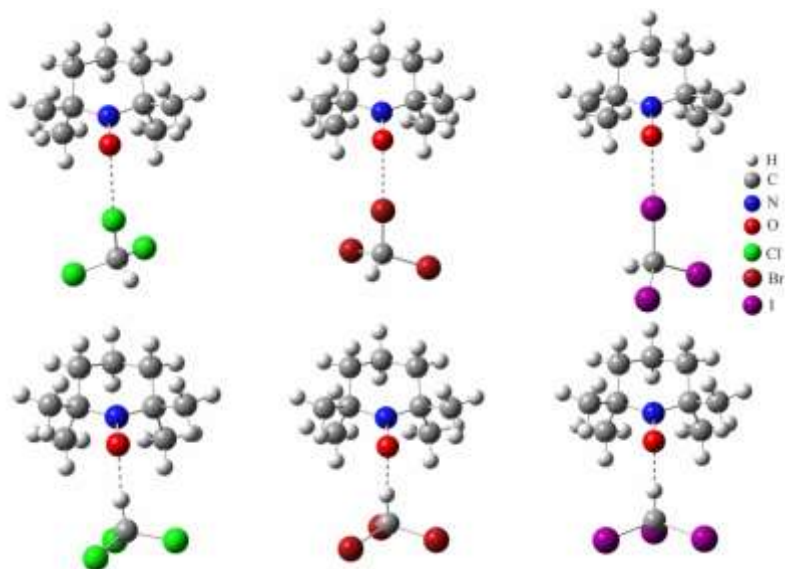


Figure 1-11. Structures of TEMPO•••CHX₃ optimized by wB97XD/aug-cc-pVDZ(-PP).²⁹

1.4 HyB/HaB Complementarity and Competition in Solid State

Although HaB can frequently dominate the crystal structures formed with weaker noncovalent interactions, it is generally of the same strength as HyB. It can compete with or cooperate with HyB. Recently, Bruce et al. have shown the complementarity and ability of HyB and HaB to interact competitively in the preparation of several cocrystals with various heterocyclic HaB and HyB acceptor molecules. Their work suggested that the best donor, HyB or HaB, preferentially interacts with the best acceptor; cocrystals of tetrafluoroiodobenzoic acid with dithiane demonstrated the formation of self-complementary solid carboxylic acid dimers accompanied by short I---S HaB. Figure 1-12 below illustrates the competition and complementarity involving HaB and HyB interactions.

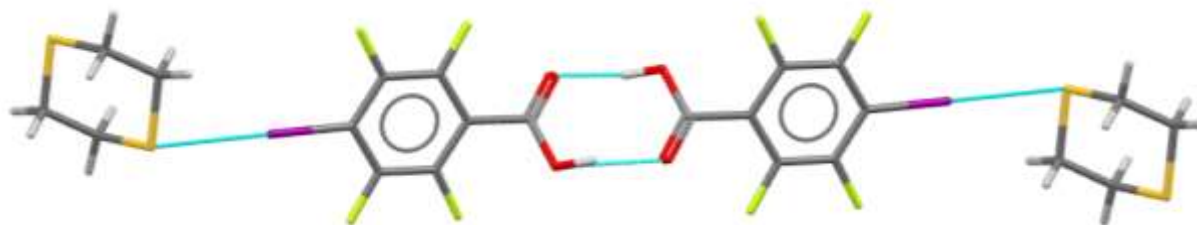


Figure 1-12. Crystal structures showing I...S halogen bonds between tetrafluoriodobenzoic acid and dithiane (CSD Refcode HIZQOY), with color codes; yellow-sulfur, purple-iodine, green-fluorine, red-oxygen, and grey-hydrogen.

Haloforms are the simplest molecules capable of both types of interactions, therefore, they have been a popular choice for chemists studying halogen and hydrogen bonds. Kochi et. al., have studied simple brominated and chlorinated molecules through co-crystallization and determined that chlorinated molecules are less likely to form halogens than brominated molecules.³⁰ Co-crystallization of iodoform with benzyltrimethylammonium iodide by the Bertolotti group revealed the affinity iodine-containing molecules possess for halogen bonding.³¹ Iodine and hydrogen atoms of CHI_3 and iodide anions are shown to form hydrogen and halogen bonds. Figure 1-13 illustrates the structure of the cocrystals formed by iodoform with benzyltrimethylammonium iodide.

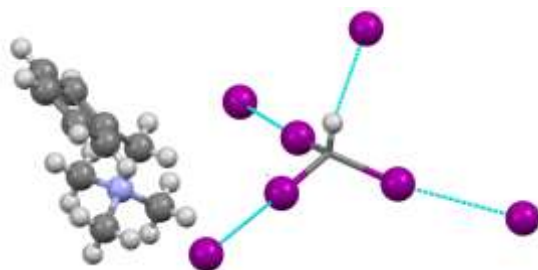


Figure 1-13. Crystal structure of benzyltrimethylammonium iodide iodoform solvate showing halogen and hydrogen bonds between CHI_3 and I^- as blue lines.³¹

Halothane, a common anesthetic, has been thought to use hydrogen bonds as an effective drug. Recently, this assumption was questioned when the Resnati group successfully co-crystallized it

with hexamethylphosphoramide. X-ray crystallography revealed halogen and hydrogen bonding between the two compounds. This finding suggests that halogen and hydrogen bonding may be responsible for the pharmaceutical activity of haloethanes. These interactions are shown in the x-ray structures display in Figure 1-14.



Figure 1-14. X-ray crystal structure of the complex between hexamethylphosphoramide and haloethane with hydrogen and halogen bonds.³²

1.5 Previous Studies on Halogen and Hydrogen Bonding in Solution

Green et al. studied whether halide size (polarizability) directly correlates with the formation of HyB or HaB bonds. They found that molecules substituted with smaller halogens preferred hydrogen bonds over halogens, whereas iodide-containing compounds preferred halogen bonds. This trend was also observed in other haloforms study. However, because of the limitations of their NMR studies, Green et al. incorrectly believed that only one type of bonding occurs in solutions.³³ Figure 1-15 below shows that HyB associations (in which NMR signals of the haloform protons are shifted to higher values) prevail in solutions of halides with CHBr_3 or CHCl_3 .

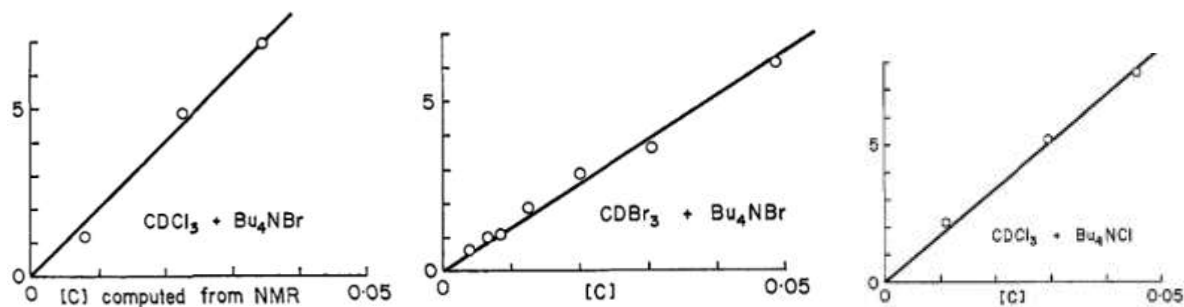


Figure 1-15. Halogen and hydrogen bonding of haloforms complexes with halides in solution.³³

Bertran et. al. studied haloforms and methylene dihalides in aza-aromatic solvents. His research concluded that a solute-solvent interaction drives HaB, but his research is more qualitative than quantitative.³⁴ The authors of the work described above stated that deriving an actual equation to determine the formation constants of halogen and hydrogen bonds coexisting was too complex. They used only ¹HNMR measurements, so they could not prove that both types of bonding occurred. Similar conclusions were obtained by Bertrán and Rodríguez based on NMR studies of the interactions of haloforms with aza-containing solvents.

UV-Vis spectroscopic techniques also have huge potential for differentiating between HaB and HyB. Rosokha et al. studied halogen- and hydrogen-bonded complexes between haloforms, such as CHI₃, CHBr₃, and CHCl₃, and (pseudo)halide anions coexisting in acetonitrile solutions and characterized them via a combination of UV-vis and NMR spectral measurements and X-ray structural and density functional theory (DFT)-based analyses. In solution, the halogen-bonded CHX₃•••A⁻ complexes displayed strong absorption bands in the UV spectra and a decreased chemical shift of the NMR signal of the haloform protons. In contrast, hydrogen bonding led to the opposite (increased) NMR signal shift and no UV-vis absorption bands of the hydrogen-bonded CHX₃•••A⁻ molecules. These findings are consistent with those of Green and Bertrán. The simultaneous multivariable treatment of the results of UV-vis and NMR titrations of CHX₃ with

A^- anions afforded the formation constants of halogen- and hydrogen-bonded complexes between these species, which existed side-by-side in the CH_3CN solutions. The relative values of the formation constants were consistent with the magnitudes of the positive potentials on the surfaces of the halogen or hydrogen atoms while also taking into account the effects of the polarization of the haloforms.³⁵ Figure 1-16 and 1-17 below shows the spectra details including UV/Vis and NMR of HaB/HyB coexisting in solution.

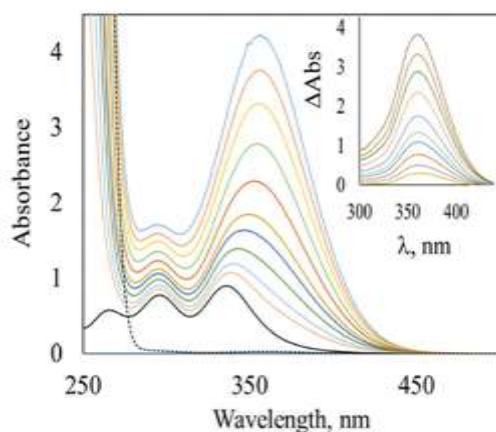


Figure 1-16. UV-Vis spectra of the solutions with a constant concentration of iodoform compound and varied concentration of iodide. The dashed line shows the spectrum of a separate Pr_4NI solution, and black solid line shows the spectrum of a separate iodoform solution. Inset: Spectra of the $[CHI_3, I^-]$ complex obtained by subtraction of the absorption of components from the spectra of their mixtures.

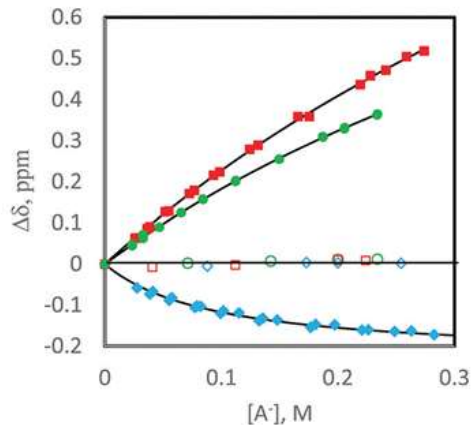


Figure 1-17. Dependencies of proton NMR shifts of CHX_3 (in CD_3CN , 22°C , relative to those in the separate molecules) on the concentration of added Pr_4NA salts. Filled symbols show proton shifts of CHI_3 (\blacklozenge), CHBr_3 (\bullet), and CHCl_3 (\blacksquare) in the presence of bromide ($\text{A} = \text{Br}$) and open symbols show the essential independence of shifts of CHI_3 (\diamond), CHBr_3 (\circ) and CHCl_3 (\square) from concentrations of (non-bonding) BF_4^- anions ($\text{A} = \text{BF}_4^-$). Concentrations of CHI_3 (5.2 mM), CHBr_3 (5.0 mM), and CHCl_3 (5.0 mM) were constant during titrations.

1.6 Electron Transfer Reaction

Because electron density can be transferred completely from the halogen bond acceptor to the halogen bond donor, it is important to understand the concept of the electron transfer reaction. Many vital processes in chemistry and biochemistry are based on electron transfer reactions. Electron transfer is the most straightforward chemical process because it involves only the movement of an electron and the bonding of atoms remains the same. This process involves the movement of electrons from the electron donor (D) to acceptor (A). Examples of electron transfer processes include respiration (the way we obtain energy from food and oxygen) and photosynthesis (the way plants produce food and oxygen), which rely entirely on electron transfer reactions. Another reason to examine electron transfer is that it is an elementary chemical reaction, and understanding it provides insights into other areas of chemistry and biochemistry.

For electrons to be transferred from one species to another, the two species must be in close proximity. If donors D and A are separate, independent species, they must first come together to form an "encounter complex" before electron transfer between D^+ and A^- can occur. This process is called an intermolecular reaction.³⁶ The shorter the distance between the donor and acceptor, the more efficient is the electron transfer. However, in many cases, the donor and acceptor are connected by a rigid molecular bridge, which eliminates the need for diffusion, and electron transfer occurs at a fixed geometric distance. In this case, we performed intramolecular electron transfer. This allowed us to study the dependence of electron transfer on the distance between the donor (D) and the acceptor (A).³⁷

Studies on the mechanism and kinetics of electron transfer began after World War II (WWII). Historically, it was initially focused on the electron transfer of inorganic species-transition metal complexes. In inorganic chemistry, the metal ions in such complexes are surrounded by ligands known as coordination spheres. In the 1950s, Henry Taube (a Nobel Prize winner for this work) showed that electrons can be transferred between metal ions via one of two primary mechanisms. One is electron transfer via the outer sphere (OS), where the coordination spheres of both ions remain intact during the process. Marcus's theory can be used to predict the rates for such reactions.³⁸

In contrast, electron transfer within the sphere (IS) begins with ligand substitution, leading to a complex in which both the ions share a ligand. This shared ligand greatly facilitates electron transfer (it provides what is known as electron coupling). Therefore, even with one additional step, the inner-sphere reaction proceeds faster than the OS analogy. After electron transfer, the ions usually separate again.³⁶ Figure 1-18 depicts the mechanisms of the electron transfer reaction.

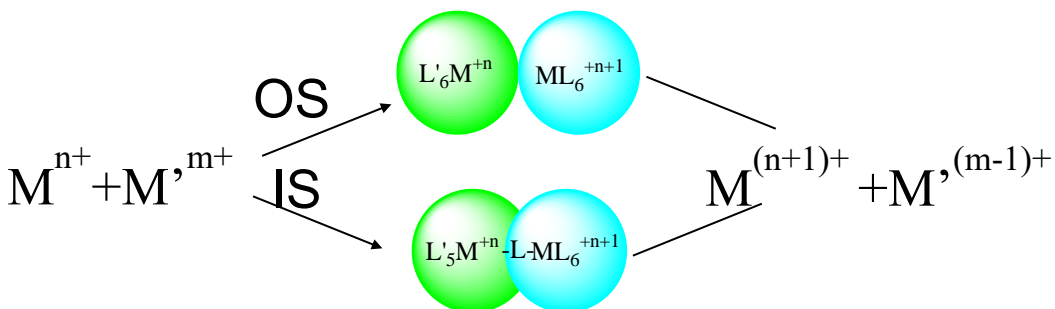


Figure 1-18. Illustration of outer-sphere and inner-sphere reaction³⁶

According to the Marcus theory, the rate constants for the intermolecular outer-sphere ET processes are calculated as follows:

$$K_{ET}^{OS} = Z e^{(\Delta G^*/RT)} \quad (1)$$

where $Z = 10^{11} \text{ M}^{-1}\text{s}^{-1}$ is the collision factor and ΔE is the activation barrier, which depends on the reorganization energy and free energy of the reaction. Figure 1-19 below illustrates the energy profile of the ET reaction, as proposed by the Marcus theory.

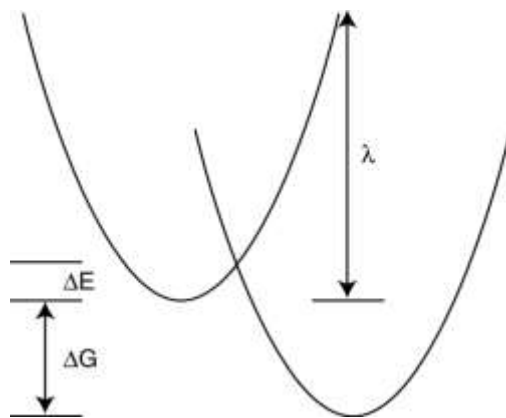


Figure 1-19. Illustration of energy diagram of Marcus Theory

These two parabolas represent the energies of the reactants and products as the nuclei move. This is a parabola because this is the relationship one would obtain if the nuclei were connected by springs (according to Hooke's Law). Marcus realized that he could solve the point of crossing between the parabolas and derive the activation energy (and thus the rate constant) from the thermodynamic parameters of the system. In this figure, ΔG is the free energy change between the reactants on the left and the products on the right, and ΔE is the activation barrier, λ is the reorganization energy, which is the energy required to force the reactants (left) to have the same nuclear configuration as the products (right) without allowing electron transfer. The activation barrier for the cross-exchange electron transfer reaction can be expressed as follows

$$\Delta G^* = \frac{(\Delta G + \lambda)^2}{4\lambda} \quad (2)$$

The Gibbs free energy (ΔG^o), on the other hand, accounts for the overall energy change associated with the electron transfer process. ΔG^o is usually calculated from the difference between the redox potentials of donors D and A as shown in equation 3 and 4.

$$\Delta E^o = E^o(D^+) - E^o(A^-) \quad (3)$$

$$\Delta G^o = -F\Delta E^o \quad (4)$$

where F is the Faraday constant.³⁷

Besides the reorganization energy and Gibbs free energy of the reaction, another factor that affects the rate of a reaction is known as coupling element. The coupling element represents the strength of the interaction between the electronic states of the donor and acceptor molecules involved in the electron transfer process. It arises from the overlap of their wavefunctions and determines the probability of electron transfer occurring between the two species. The coupling element affects

both the reorganization energy and the Gibbs free energy of the reaction, playing a significant role in determining the efficiency and rate of electron transfer processes.

The ground-state ET potential-energy surface is evaluated using a model called Marcus Hush, where the energies of the initial and final diabatic states and the coupling element are taken into account. This ground-state ET potential-energy surface is evaluated as:

$$E_{\text{GS}} = (H_{\text{aa}} + H_{\text{bb}})/2 - ((H_{\text{bb}} - H_{\text{aa}})^2 + 4H_{\text{ab}}^2)^{1/2}/2 \quad (5)$$

Where $H_{\text{aa}} = \lambda X^2$ and $H_{\text{bb}} = \Delta G_{\text{ET}}^0 + \lambda (X - 1)^2$ are energies of the initial and final states at each point along the ET reaction coordinate, from $X = 0$ to $X = 1$, and H_{ab} is coupling element, can be determined from the spectral and structural characteristics of the redox-systems via the Hush expression given in eq 6 below, and as it increases, the barrier for electron transfer decreases, up to complete electron delocalization in the systems with $H_{\text{ab}} \geq \lambda/2$.

$$H_{\text{ab}} = 0.0206 (\nu_{\text{CT}} \Delta \nu_{1/2} \epsilon_{\text{CT}})^{1/2} / r_{\text{DA}} \quad (6)$$

Where ν_{CT} , $\Delta \nu_{1/2}$, and ϵ_{CT} are minimum, full-width at half maximum, and the extinction coefficient of the absorption band related to optical ET between the redox centers and r_{DA} is their separation.³⁹

1.7 Halogen Bond and Electron Transfer Reaction

Halogen bonding can play a significant role in electron transfer reactions. Little work has been done on how halogen bonding affects the ET reaction. Rosokha et. al., studied the role of halogen bonding in redox reactions of tetrabromomethane and tribromonitromethane with tetramethyl-p-phenylenediamine (TMPD). This study showed that halogen bonding plays an important role in the redox reactions of tetrabromomethane and tribromonitromethane with TMPD by significantly lowering the activation barriers for electron transfer. The rate constants of these processes can be evaluated from the spectral, structural, and thermodynamic characteristics of halogen-bonded

associates. The studied also discusses the isolation of pre-reactive complexes and analysis of kinetics of redox reactions to understand the role of halogen bonding in these processes.⁴⁰

Another work by Rosokha involved experimental and computational studies of halogen-bonded complexes formed between bromosubstituted electrophiles and halide anions. This work also discusses the role of electron transfer in the chemical transformation of halogen-containing compounds. At the limit of the strongest electron donor-acceptor pairs, the formation of the halogen-bonded complexes was followed by the oxidation of iodide to triiodide, which occurs through an inner-sphere electron transfer process. Figure 1-20 below shows the ET reaction via halogen bonded complex.⁴¹

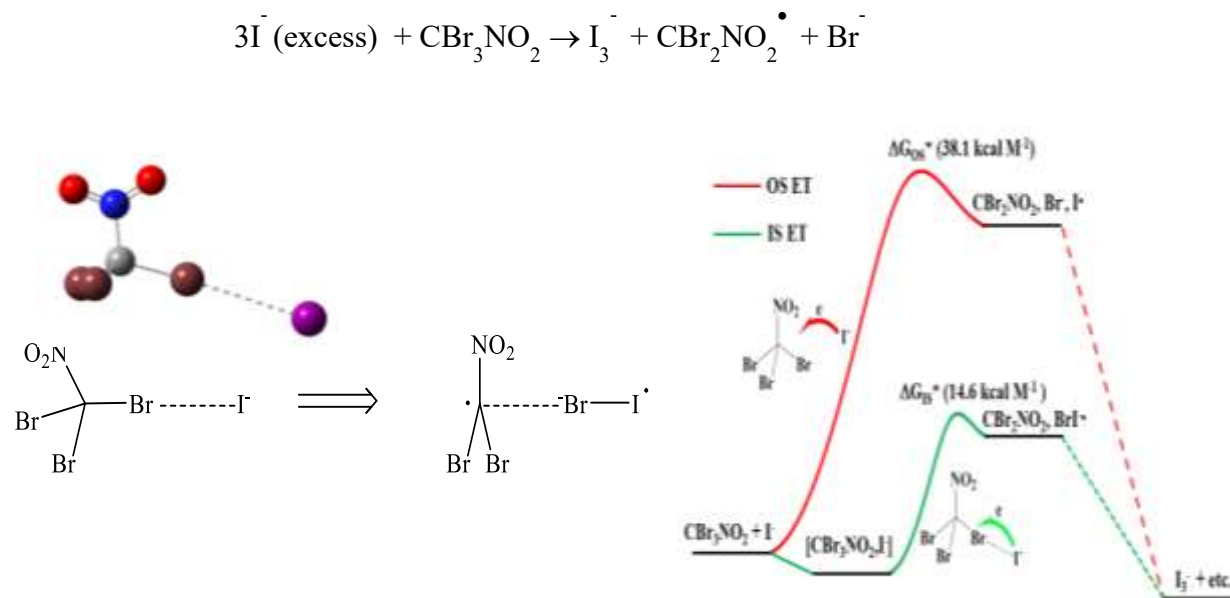


Figure 1-20. Inner sphere electron transfer via a halogen-bonded complex between tribromonitromethane and iodide anion.⁴⁰

The Marcus-Hush two-state model stated above was used to evaluate the ground-state ET potential-energy surface between tribromonitromethane and iodide in the precursor complex. The electronic coupling element was calculated to be $8.9 \text{ kcal mol}^{-1}$ based on the spectral and structural characteristics of the halogen-bonded $[\text{CBr}_3\text{NO}_2, \text{I}^-]$ complex.

In summary, it has been shown in previous studies that substances containing both halogen and hydrogen substituents form halogen and hydrogen bonds, and that such bonds can be easily identified in solid-state X-ray structures. It is much more difficult to determine the interactions in solution. In addition, previous studies have established that halogen bonds play an important role in electron-transfer reactions. The uniqueness of this project is based on the fact that we consider our studies in neutral systems (i.e., haloforms and amines), different from the previous studies in the literature involving haloforms and anionic systems (i.e., halides).

The goals of this study are as follows:

- 1) To separate halogen- and hydrogen-bonded complexes between haloforms (CHX_3) and amines in solution.
- 2) To characterize these complexes quantitatively in solution using experimental methods such as UV-Vis/NMR spectral measurements and computational analyses, and in the solid-state using X-ray structural analysis.
- 3) To study the role of halogen bonds in electron-transfer reactions between iodine (I_2) and amines.

CHAPTER 2

EXPERIMENTAL SECTION

2.1 Materials

Most halogen and hydrogen bond acceptors, aliphatic amines including DABCO, and triethylamine, aromatic amines (such as DMA, DMABr, DMAF, DMACN, TMPD, pMeODMA, and mMeODMA), TBAX, and heterocyclic compounds including PTZ and MPTZ, HaB and HyB bond donors, these include iodine, bromoform, iodoform, and chloroform were purchased commercially. The (halo)imidazolium compounds also used in this project were provided by Dr. Huber in Germany. Some of these reagents were purified by sublimation and recrystallization before use. Dichloromethane, hexane and acetonitrile (HPLC grade) were also purchased commercially.

2.2 X-ray Crystallography Analysis

Cooling acetonitrile solutions containing equimolar quantities of iodoform and either TMPD or DABCO resulted in cocrystals suitable for X-ray structural measurements. CHI₃ and DABCO crystals were formed by dissolving 21.1 mg of CHI₃ in 2mL of acetonitrile and 6.2 mg of DABCO in 2mL of acetonitrile; the two solutions were then combined and slowly cooled to 0°C by placing them in a Styrofoam container that was then placed in the freezer. Similar crystallization was achieved by cooling acetonitrile solutions containing equimolar quantities of TMPD and other aromatic amines, I₂ and MPTZ crystals, and I₂ and pMeODMA. The X-ray structural analysis of these crystals was performed by Dr. Mathias Zeller at Purdue University.

Single crystals of the iodoform complexes with DABCO and TMPD were analyzed using a Bruker Quest diffractometer with kappa geometry, a copper radiation I-m-S micro source X-ray tube ($\lambda = 1.54178 \text{ \AA}$), laterally graded multilayer (Goebel) mirror single crystal for monochromatization, and a Photon2 CMOS area detector. Examination and data collection were performed at 150 K. Single crystals of all other complexes were coated with oil and quickly transferred to the goniometer head of a Bruker Quest diffractometer with a fixed chi angle, molybdenum radiation-sealed tube fine-focus X-ray tube ($\lambda = 0.71073 \text{ \AA}$), single-crystal curved graphite incident beam monochromator, and Photon100 CMOS area detector. Both instruments were equipped with Oxford Cryosystems low-temperature devices, and examinations and data collection were performed at 150 K. Data were collected, reflections were indexed and processed, and the files were scaled and corrected for absorption using APEX3.26. The space groups were assigned, and the structures were solved by direct methods using XPREP within the SHELXTL suite of programs and refined by full-matrix least-squares against F² with all reflections using Shelxl2016 with the graphical interface Shelxle. Details of the crystallography, data collection, and structural refinement are listed in Table 2-1.

Table 2-1. Crystallography, data collection, and refinement details.

	CHI ₃ ·DABCO	CHI ₃ ·TMPD	CHI ₃ ·TMPD	I ₂ ·MPTZ	I ₃ ·pMeODMA
Chemical formula	C ₆ H ₁₂ N ₂ ·CHI ₃	C ₁₀ H ₁₆ N ₂ ·2(CHI ₃)	C ₁₃ H ₂₀ I ₃ N ₃	6(C ₁₃ H ₁₁ NS)·3.542(I ₅)·1.458(I ₃)·4.458(I ₂)	C ₉ H ₁₃ NO·I ₃
<i>M_r</i>	505.89	951.68	599.02	5213.62	531.90
Crystal system, space group	Orthorhombic, <i>Pnma</i>	Triclinic, <i>P</i> 1	Orthorhombic, <i>Pnma</i>	Monoclinic, <i>C2/c</i>	Triclinic, <i>P</i> 1
Temperature (K)	150	150	150	150	150
<i>a</i> , <i>b</i> , <i>c</i> (Å)	16.4635 (13), 10.6079 (9), 7.3574 (6)	6.6114 (3), 9.6487 (5), 9.8861 (5)	10.5562 (5), 15.1118 (6), 11.6277 (5)	45.7526 (17), 11.4010 (4), 25.7627 (10)	8.2424 (5), 9.7733 (6), 10.1844 (6)
α , β , γ (°)		63.578 (2), 83.094 (3), 74.633 (3)		119.171 (1)	104.701 (3), 98.522 (3), 108.746 (3)
<i>V</i> (Å ³)	1284.92 (18)	544.58 (5)	1854.89 (14)	11734.1 (8)	727.43 (8)
<i>Z</i>	4	1	4	4	2
Radiation type	Mo <i>K</i> α	Mo <i>K</i> α	Mo <i>K</i> α	Mo <i>K</i> α	Mo <i>K</i> α
μ (mm ⁻¹)	7.26	8.55	5.05	8.31	6.42
Crystal size (mm)	0.25 × 0.23 × 0.18	0.21 × 0.20 × 0.13	0.32 × 0.25 × 0 .16	0.12 × 0.11 × 0.03	0.45 × 0.27 × 0.04
<i>T_{min}</i> , <i>T_{max}</i>	0.432, 0.747	0.500, 0.747	0.539, 0.747	0.054, 0.100	0.392, 0.747
No. of measured, independent and observed [<i>I</i> > 2σ(<i>I</i>)] reflections	13583, 3209, 2702	13429, 4038, 3603	52270, 3646, 3302	98833, 17954, 13927	25741, 5523, 4619
<i>R_{int}</i>	0.040	0.037	0.043	0.047	0.056
(sin <i>q/l</i>) _{max} (Å ⁻¹)	0.833	0.771	0.769	0.715	0.770
<i>R</i> [<i>F</i> ² > 2σ(<i>F</i> ²)], <i>wR</i> (<i>F</i> ²), <i>S</i>	0.037, 0.082, 1.06	0.022, 0.046, 1.05	0.013, 0.028, 1. 06	0.029, 0.062, 1.03	0.037, 0.106, 1.07
No. of reflections	3209	4038	3646	17954	5523
No. of parameters	65	94	98	568	131
<i>D</i> _{pmax} , <i>D</i> _{pmin} (e Å ⁻³)	2.58, -2.25	1.79, -1.73	0.50, -0.43	1.42, -1.48	2.17, -1.73

2.3 UV-Vis Spectroscopic Measurements

UV-Vis measurements were carried out in open air on an Agilent Cary 5000 UV-Vis-NIR spectrophotometer in dry (HPLC grade) acetonitrile with a 1 mm cuvette at room temperature. The

trihalomethane compounds (haloforms) were dissolved with ACN to make 5 mL of (0.01-0.02) M solutions in a volumetric flask, and the amines used for that trial were dissolved in ACN to make up 3mL of (1.2-1.6) M in a volumetric flask. A series of solutions were made up to 1mL in vials containing trihalomethane compounds (0.5mL) with varying concentrations of amines. Each was run directly after preparation at 200 nm–600 nm. The iodoform decomposes with light, so it was protected from it by dimming the room, and the stock solutions were wrapped in foil. The typical volumes of the stock solutions used in the series of measurements are listed in Table 2-2.

Table 2-2: Example of the volumes used for each trial in mL for a typical UV-Vis experiment

Trial	1	2	3	4	5	6	7	8	9	10
HAB donor	0	0.5	0	0.5	0.5	0.5	0.5	0.5	0.5	0.5
HAB acceptor	0	0	0.5	0.5	0.4	0.33	0.25	0.17	0.1	0.05
Acetonitrile	1	0.5	0.5	0	0.1	0.17	0.25	0.33	0.4	0.45

2.4 ¹H NMR Spectroscopic Measurements

NMR measurements were performed on a 400 MHz spectrometer in deuterated acetonitrile with an internal TMS standard using NMR tubes at room temperature. The haloform compounds were dissolved in ACN-D₃ to make 3 mL of 0.02 M solutions in a volumetric flask, and the amines used for those trials were dissolved in ACN-D₃ to make up 3mL of 1.2 M in a volumetric flask. A series of NMR solutions were prepared, which comprised small vials containing 0.25mL of the haloform solution and varying concentrations of the amines. The iodoform decomposed in light; therefore, the room was dimmed, and the stock solutions were wrapped in foil. The typical volumes of the stock solutions used in the series of measurements are listed in Table 2-3.

Table 2-3: Example of volumes used for each trial in mL for a typical ^1H NMR experiment.

Trial	1	2	3	4	5	6	7	8	9
HaB Donor	0.25	0	0.25	0.25	0.25	0.25	0.25	0.25	0.25
HaB Acceptor	0	0.25	0.25	0.2	0.165	0.125	0.085	0.05	0.025
Acetonitrile	0.25	0.25	0	0.05	0.085	0.125	0.165	0.2	0.225

2.5 Gaussian Computations

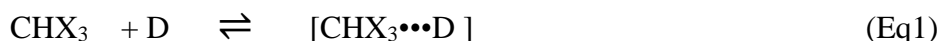
The geometries of the HaB and HyB complexes were optimized by M062x/def2tzvpp DFT calculations. The complexes were drawn in Gauss View and computations were performed using the Gaussian09 program suite. The complexes were optimized in acetonitrile (with the PCM model) using an ultrafine grid and had the maximum cycle set to 128 for the complexes containing DABCO. Once the complexes were optimized, HaB and HyB bond lengths and angles were determined. The bonding energy, ΔE , of the HaB and HyB complexes was also determined by taking the energy of the complex (E_{comp}), including the zero-point energy (ZPE), and subtracting the electronic energy and ZPE of the HaB acceptor (E_a), which is an amine or DABCO, from the haloform species (E_x).

$$\Delta E = E_{\text{comp}} - (E_x + E_a)$$

After all complexes were optimized, UV-Vis and NMR spectra were calculated via TD-DFT and GIAO, respectively, in acetonitrile. The ϵ and λ values were determined from the UV-Vis spectra, while the shift for the hydrogen peaks was determined by subtracting the peaks of the halogenated species from their corresponding complex peaks. Electrostatic potential and electron density cube files were created using the medium texture for the haloform species by themselves, and V_{max} on the surface was found in the area with the most positive potential for both the hydrogen and halogen portions of the compound. Single-point calculations were performed for complexes containing amines and the polarizations of the HyB and HaB complexes were determined

2.6 Calculation of K and ϵ Values of the HaB and HyB Complexes

The extinction coefficients for the [CHX₃, D] complexes were first calculated using the Benesi-Hildebrand procedure, and then through regression analysis. Based on previous studies, it was assumed that only one type of bond formation of a 1:1 complex was formed in solution, such that all other formations could be excluded.



The effective formation constant (K_{eff}) can be expressed as

$$K_{\text{eff}} = C_{\text{com}} / ((C_{\text{D}}^{\circ} - C_{\text{com}})(C_{\text{A}}^{\circ} - C_{\text{com}})) \quad (\text{Eq2})$$

where the concentration of the complex is C_{com} and the initial concentrations of CHX₃ and D are C_{D}° and C_{A}° , respectively. When $C_{\text{A}}^{\circ} \gg C_{\text{D}}^{\circ}$, $C_{\text{A}}^{\circ} - C_{\text{com}} \approx C_{\text{A}}^{\circ}$. Therefore, $K_{\text{eff}} = C_{\text{com}} / ((C_{\text{D}}^{\circ} - C_{\text{com}})C_{\text{A}}^{\circ})$. Thus,

$$K_{\text{eff}}(C_{\text{D}}^{\circ} - C_{\text{com}})C_{\text{A}}^{\circ} - C_{\text{com}} = 0 \quad (\text{Eq3})$$

Or

$$C_{\text{com}} = K_{\text{eff}}C_{\text{D}}^{\circ}C_{\text{A}}^{\circ} / (K_{\text{eff}}C_{\text{D}}^{\circ} + 1) \quad (\text{Eq4})$$

Using the Benesi-Hildebrand equation $\Delta\text{Abs} = \epsilon l C_{\text{com}}$, where the absorbance of the complex at a particular wavelength is ΔAbs , the extinction coefficient is ϵ , and the path length is l , the previous equation can be rearranged as:

$$C_{\text{D}}^{\circ} / \Delta\text{Abs} = 1/(\epsilon l) + 1/K_{\text{eff}} \times 1/[C_{\text{A}}^{\circ}] \quad (\text{Eq5})$$

Where $K_{\text{UV}}^{\text{eff}}$ is the effective UV-Vis formation constant. When using the Benesi-Hildebrand procedure, reliable results can only occur when one of the reactants, in this case, the amines, is added in substantial excess and the other reactant's complexation is in the 20-80% range. Thus, to verify the values of $K_{\text{UV}}^{\text{eff}}$ and, as well as to determine $K_{\text{NMR}}^{\text{eff}}$ (effective formation constant of the ¹HNMR) and (hydrogen peak shift, where the difference between the ppm of the CHX₃ proton in

the presence of an infinite concentration of amine and that of the separate CHX₃ was considered), regression analysis of both the UV-Vis and NMR data were run without using the assumptions made by the Benesi-Hildebrand method. This leads to Eq6:

$$C_{\text{com}} = (C^{\circ}_{\text{A}} + C^{\circ}_{\text{D}} + 1/K_{\text{eff}}) \pm \{((C^{\circ}_{\text{A}} + C^{\circ}_{\text{D}} + 1/K_{\text{eff}})^2 - 4C^{\circ}_{\text{A}}C^{\circ}_{\text{D}})^{0.5}\} / 2 \quad (\text{Eq6})$$

The UV-Vis absorption intensity changes are described as follows:

$$\Delta\text{Abs} = \epsilon l \times C_{\text{com}} = \epsilon l \times (C^{\circ}_{\text{A}} + C^{\circ}_{\text{D}} + 1/K_{\text{eff}}) - \{((C^{\circ}_{\text{A}} + C^{\circ}_{\text{D}} + 1/K_{\text{eff}})^2 - 4C^{\circ}_{\text{A}}C^{\circ}_{\text{D}})^{0.5}\} / 2 \quad (\text{Eq7})$$

Moreover, the shifting of the hydrogen peak for ¹HNMR can be written as

$$\Delta\delta = \Delta\delta_{\infty} C_{\text{com}} / C^{\circ}_{\text{D}} = (\Delta\delta_{\infty} / C^{\circ}_{\text{D}}) \times / 2 \quad (\text{Eq8})$$

Using ϵ and $K_{\text{UV}}^{\text{eff}}$ as adjustable parameters, the UV-Vis data were fitted, as shown in Eq7 using Origin Pro. Using $K_{\text{NMR}}^{\text{eff}}$ and $\Delta\delta_{\infty}$ as adjustable parameters, the NMR results were also fitted.

However, the spectral and computational data indicated that the interaction of compounds containing halogen and hydrogen substituents with nucleophile A resulted in the formation of both HaB and HyB complexes. These processes are characterized by equilibria constants K_{HaB} and K_{HyB} , respectively.



Analysis of the experimental data indicated that the interaction of halogenated molecules (CHX₃) with anions produces, under experimental conditions, predominantly 1:1 complex (either HaB or HyB).⁴ Their formation constants are expressed as

$$K_{\text{HaB}} = C_{\text{HaB}} / ((C^{\circ}_{\text{D}} - C_{\text{HaB}} - C_{\text{HyB}})(C^{\circ}_{\text{A}} - C_{\text{HaB}} - C_{\text{HyB}})) \quad (\text{Eq11})$$

$$K_{\text{HyB}} = C_{\text{HyB}} / ((C^{\circ}_{\text{D}} - C_{\text{HaB}} - C_{\text{HyB}})(C^{\circ}_{\text{A}} - C_{\text{HaB}} - C_{\text{HyB}})) \quad (\text{Eq12})$$

C_{HaB} is the equilibrium concentration of the HaB complexes, and C_{HyB} is the same for the HyB complexes. Using this information, Eq11 and Eq12 can then be written as

$$K_{\text{HaB}}((C^{\circ}_{\text{D}} - C_{\text{HaB}} - C_{\text{HyB}})(C^{\circ}_{\text{A}} - C_{\text{HaB}} - C_{\text{HyB}})) = C_{\text{HaB}} \quad (\text{Eq13})$$

$$K_{\text{HyB}}((C^{\circ}_{\text{D}} - C_{\text{HaB}} - C_{\text{HyB}})(C^{\circ}_{\text{A}} - C_{\text{HaB}} - C_{\text{HyB}})) = C_{\text{HyB}} \quad (\text{Eq14})$$

Thus $(C^{\circ}_{\text{D}} - C_{\text{HaB}} - C_{\text{HyB}})(C^{\circ}_{\text{A}} - C_{\text{HaB}} - C_{\text{HyB}}) = C_{\text{HaB}}/K_{\text{HaB}} \quad (\text{Eq15})$

$$(C^{\circ}_{\text{D}} - C_{\text{HaB}} - C_{\text{HyB}})(C^{\circ}_{\text{A}} - C_{\text{HaB}} - C_{\text{HyB}}) = C_{\text{HyB}}/K_{\text{HyB}} \quad (\text{Eq16})$$

Or $C_{\text{HyB}} / K_{\text{HyB}} = C_{\text{HaB}}/K_{\text{HaB}} \quad (\text{Eq17})$

$$C_{\text{HaB}} = K_{\text{HaB}} C_{\text{HyB}} / K_{\text{HyB}} \quad (\text{Eq18})$$

$$C_{\text{HyB}} = K_{\text{HyB}} C_{\text{HaB}}/K_{\text{HaB}} \quad (\text{Eq19})$$

Using this equation, a substitution can occur in Eq15, and after it is rearranged, the following equation is obtained:

$$(C^{\circ}_{\text{D}} - C_{\text{HaB}}(1 + K_{\text{HyB}}/K_{\text{HaB}}))(C^{\circ}_{\text{A}} - C_{\text{HaB}}(1 + K_{\text{HyB}}/K_{\text{HaB}})) - C_{\text{HaB}}/K_{\text{HaB}} = 0 \quad (\text{Eq20})$$

$$C^{\circ}_{\text{A}}C^{\circ}_{\text{D}}/(1 + K_{\text{HyB}}/K_{\text{HaB}}) - C_{\text{HaB}}(C^{\circ}_{\text{A}} + C^{\circ}_{\text{D}} + 1/(K_{\text{HaB}} + K_{\text{HyB}})) + C_{\text{HaB}}^2(1 + K_{\text{HyB}}/K_{\text{HaB}}) = 0 \quad (\text{Eq 20})$$

$$C_{\text{HaB}} = (2(1 + K_{\text{HyB}}/K_{\text{HaB}})) \quad (\text{Eq22})$$

$$C_{\text{HyB}} = (2(1 + K_{\text{HaB}}/K_{\text{HyB}})) \quad (\text{Eq23})$$

This leads to the following:

$$\Delta\text{Abs} = \varepsilon l \times C_{\text{HaB}} = \varepsilon l \times \{((C^{\circ}_{\text{A}} + C^{\circ}_{\text{D}} + 1/(K_{\text{HaB}} + K_{\text{HyB}})) - (((C^{\circ}_{\text{A}} + C^{\circ}_{\text{D}} + 1/(K_{\text{HaB}} + K_{\text{HyB}}))^2 - 4C^{\circ}_{\text{A}} - C^{\circ}_{\text{D}})^{0.5}) / (2(1 + K_{\text{HyB}}/K_{\text{HaB}}))\} \quad (\text{Eq 24})$$

And:

$$\begin{aligned} \Delta\delta &= \Delta\delta_{\text{HaB}}/C^{\circ}_{\text{D}} \times C_{\text{HaB}} + \Delta\delta_{\text{HyB}}/C^{\circ}_{\text{D}} \times C_{\text{HyB}} = \\ &= \Delta\delta_{\text{HaB}}/C^{\circ}_{\text{D}} \times \{((C^{\circ}_{\text{A}} + C^{\circ}_{\text{D}} + 1/(K_{\text{HaB}} + K_{\text{HyB}})) - (((C^{\circ}_{\text{A}} + C^{\circ}_{\text{D}} + 1/(K_{\text{HaB}} + K_{\text{HyB}}))^2 - 4C^{\circ}_{\text{A}} - C^{\circ}_{\text{D}})^{0.5}) / (2(1 + K_{\text{HyB}}/K_{\text{HaB}}))\} \\ &+ \Delta\delta_{\text{HyB}}/C^{\circ}_{\text{D}} \times \{((C^{\circ}_{\text{A}} + C^{\circ}_{\text{D}} + 1/(K_{\text{HaB}} + K_{\text{HyB}})) - (((C^{\circ}_{\text{A}} + C^{\circ}_{\text{D}} + 1/(K_{\text{HaB}} + K_{\text{HyB}}))^2 - 4C^{\circ}_{\text{A}} - C^{\circ}_{\text{D}})^{0.5}) / (2(1 + K_{\text{HaB}}/K_{\text{HyB}}))\} \end{aligned} \quad (\text{Eq25})$$

Using Eq24 and Eq25, a simultaneous nonlinear fitting for the dependencies of ΔAbs and $\Delta\delta$ on the concentration of (amines), D can be performed in OriginPro. For the fittings, the concentration of the anion was used as an independent variable, whereas the values of ΔAbs and $\Delta\delta$ were the dependent variables. K_{HyB} , K_{HaB} , and ε were used as adjustable parameters, and the ((HaB and ((HyB) found using DFT calculations), and the concentrations of haloform compounds were used as constants. The K_{HaB} and K_{HyB} values were determined using these parameters.

RESULTS AND DISCUSSION

CHAPTER 3. HALOGEN- AND HYDROGEN-BONDED COMPLEXES OF HALOFORMS WITH ALIPHATIC AND AROMATIC AMINES

3.1 X-ray Crystallographic Analysis

X-ray crystallography is a powerful technique that allows scientists to determine the three-dimensional structures of molecules and materials at the atomic level. Crystals were obtained to determine whether HaB and HyB formed in the solid state. Cooling acetonitrile solutions containing equimolar quantities of iodoform and either TMPD or DABCO led to the formation of cocrystals suitable for X-ray structural measurements. The crystal structures show HaB and HyB in the structure of iodoform with DABCO and HaB in the structure of iodoform with TMPD. Two variations of the crystal structures of CHI_3 with TMPD was seen in the X-ray results, one is 1:1 (A), and the other one is 1:2 (B), the former was done in acetonitrile and the second one (B) was done without acetonitrile. The structure of CHI_3 with DABCO is 1:1 (C). We attempted to prepare crystals for other amines with various haloforms; unfortunately, we did not obtain crystals. Figure 3-1 illustrates the X-ray structures of the iodoform co-crystals of TMPD and DABCO, showing the HaB/HyB interactions.

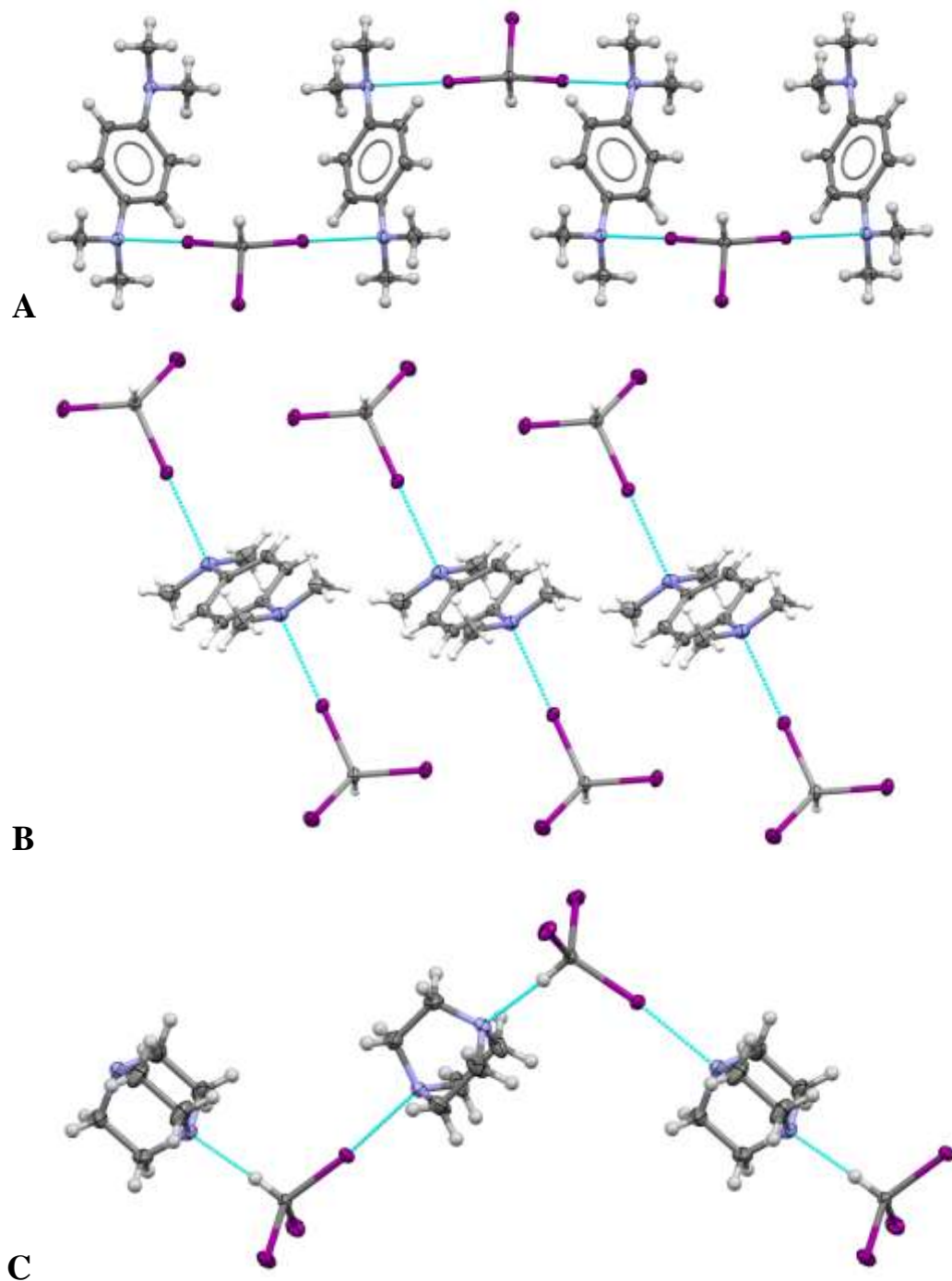


Figure 3-1. X-ray structures of iodoform co-crystals with TMPD (A:1:1, B:2:1) and DABCO (C) showing alternating halogen (and hydrogen) bonded zigzag chains represented with the blue lines.

In the crystals formed by CHI₃ and TMPD, the halogen bond between the two iodine substituents in each CHI₃ and the two amino groups in each TMPD formed chains of iodoform-TMPD. The distance between the halogen substituents and the nitrogen in the amine was approximately 22 % smaller than the sum of the van der Waals radii of these atoms, and the C-I-N angles were nearly linear (177.9°), which is typical for halogen bonding. In contrast, the DABCO molecules were linked to the iodoform by I•••N halogens and H•••N hydrogens. The HyB and HaB bonds were nearly linear (177.1° and 174.2°, respectively) and relatively short (2.152Å and 2.756Å, respectively). Interestingly, the I•••N in the association of DABCO with iodoform was shorter than that of Br•••N distances of 2.877 Å in both the halogen and hydrogen bonds of this nucleophile with bromoform.³⁵ It indicates a significantly stronger HaB involving iodine atoms. Overall, the interaction of the iodoform with the aromatic or aliphatic amines was similar to that of the halide anions.

Determining these interactions in the solid state is quite easy, but in the solution phase, it is more challenging, and to further clarify these interactions seen in the X-ray structures, we turned in to UV-Vis and NMR studies.

3.2 UV-Vis Measurements of HaB and HyB Complex in Solution.

UV-Vis spectroscopy is a widely used technique for studying the electronic transitions in molecules and determining the formation of complex. In the context of halogen-bond complexes, UV-Vis spectroscopy can provide valuable insights into the nature and strength of the interaction between the halogen atom and the electron-rich partner. UV-Vis spectroscopic measurements were performed to examine the competition between these interactions in solution.

By monitoring changes in the absorption spectrum of the complex, one can gain information about the absorption wavelengths, coefficient of absorptivity, and equilibrium constants of the complexes can be obtained. We measured the UV-Vis spectra of the complexes formed between the haloforms and aliphatic amines (such as DABCO and TEA) and aromatic amines (including TMPD, DMA, mMeODMA, DMAF, DMACN, and DMABr). First, the complexes of the haloforms with DABCO were analyzed. Although the UV-Vis spectrum of DABCO is transparent at > 300 nm, the addition of this amine to an acetonitrile solution containing iodoform resulted in an increase in absorption in the 300 – 400 nm range. Subtraction of the absorption of each component showed that this increase was related to the appearance of a pair of close absorption bands (Figure 3-2). In solutions with a constant concentration of iodoform, the intensity of these bands increased with increasing concentration of DABCO. The results of UV-Vis measurements of the solution series with a constant concentration of CHI_3 and various concentrations of DABCO are shown in Figure 3-2.

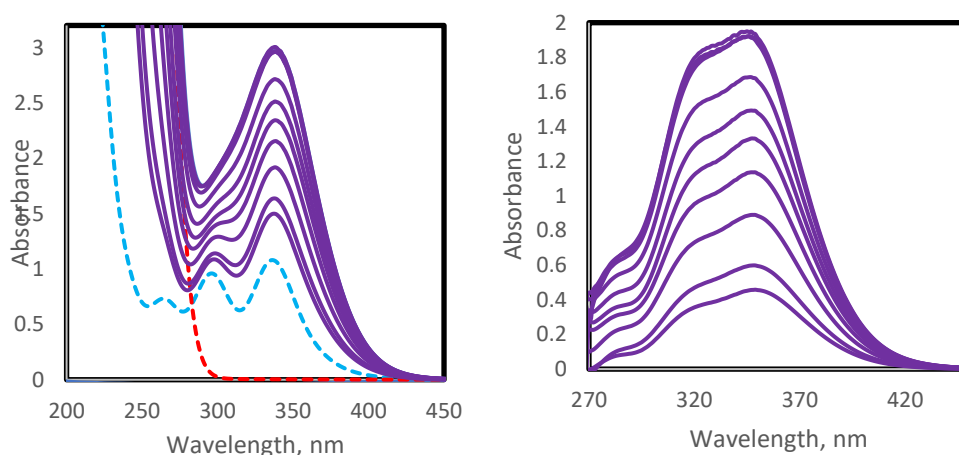


Figure 3-2. (Left) Spectra of solutions with constant concentrations of CHI_3 (0.01M) and various concentrations of 1,4-diazabicyclo[2,2,2]octane (DABCO). The spectra of the solutions of the individual reactants are shown as dashed blue (CHI_3) and red (DABCO) lines. (Right) Spectra of the complexes obtained by subtraction of the absorption of components from the spectra of their mixtures.

The addition of DABCO to the bromoform also resulted in the appearance of a new absorption band in the UV-Vis spectra (Figure 3-3). This new band is substantially blue-shifted compared to that observed for CHI_3 , and it was partially overshadowed by the absorption of DABCO itself. In comparison, solutions of DABCO and CHCl_3 did not show any new absorption beyond 280 nm, and the strong absorption of DABCO hindered measurements below this wavelength. Figure 3-3 shows the UV-Vis spectra of CHBr_3 with DABCO.

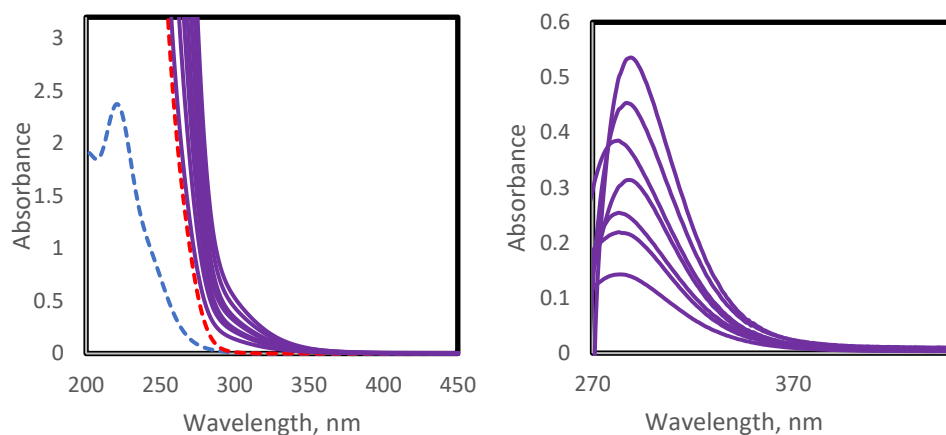


Figure 3-3. (Left) Spectra of solutions with a constant concentration of CHBr_3 (0.01M) and various concentrations of DABCO. The spectra of the solutions of the individual reactants are shown as dashed blue (CHBr_3) and red (DABCO) lines. (Right) Spectra of the complexes obtained by subtraction of the absorption of components from the spectra of their mixtures.

Similar UV-Vis measurements of the interactions of the haloforms with TMPD were hindered by the strong absorption of TMPD in the 200-380 nm range. As such, only part of the new absorption of the complex of TMPD with CHI_3 was observed at > 380 nm, and the corresponding band of the complex with CHBr_3 was apparently overshadowed by the absorption of TMPD. The same appearances of new absorptions were observed upon addition of other N,N-dimethylanilines or triethylamine to CHI_3 (Figures S1-S6 in the Supporting Information).

The UV-Vis spectra of CHI_3 with TMPD is shown in Figure 3-4 below.

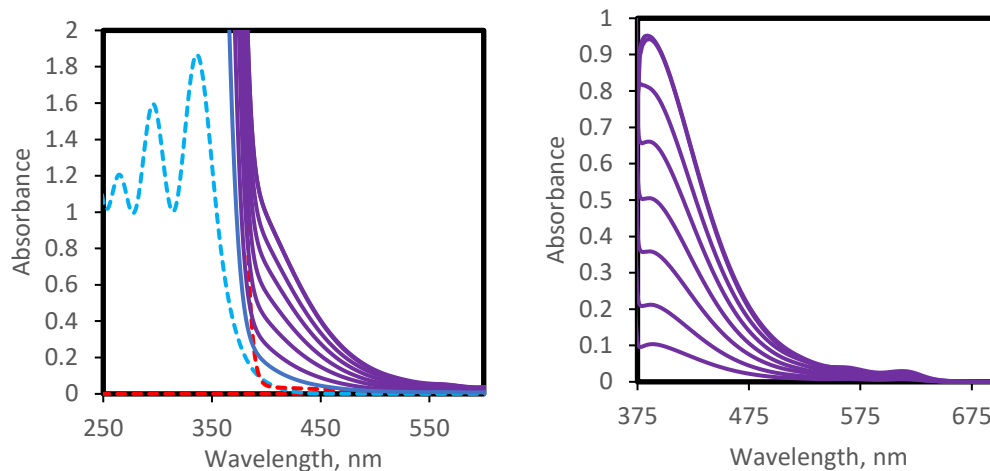


Figure 3-4. (Left) Spectra of solutions with constant concentrations of CHI_3 (0.01M) and various concentrations of tetramethyl-p-phenylenediamine (TMPD). The spectra of the solutions of the individual reactants are shown by the dashed blue (CHI_3) and red (TMPD) lines. (Right) Spectra of the complexes obtained by subtracting the absorption of components from the spectra of their mixtures.

Overall, the increasing absorption bands in the results suggested that HaB bonded complexes are formed in the solution. Because there is a combination of HaB and HyB complexes in the solution, we used ^1H NMR to further differentiate the HaB and HyB complexes.

3.3 ^1H NMR Measurement of HaB and HyB Complex in Solution.

^1H NMR (proton nuclear magnetic resonance) spectroscopy is a powerful analytical technique used to study the structure and reaction of molecules. In the analysis of halogen and hydrogen-bonded complexes, ^1H NMR provides valuable information about the interaction of the hydrogens by observing changes in the chemical shifts. Complex formation was confirmed using a series of ^1H NMR spectra. The addition of DABCO to the solution of CHI_3 in deuterated acetonitrile resulted in a shift in the signal of the proton of the haloform to lower ppm values (Figure 3-5) indicating increased shielding of this proton. A similar addition of DABCO to bromoform or chloroform produced a shift in the proton signal to higher ppm values (Figure 3-5). These results are consistent with earlier studies on the interaction of the haloform with halide anions,³⁵ and suggest a

prevalence of HaB complexes in solutions of iodoforms with aliphatic amines, and a domination of HyB in similar solutions with bromoform or chloroform. This is shown in Figures 3-5 shown below.

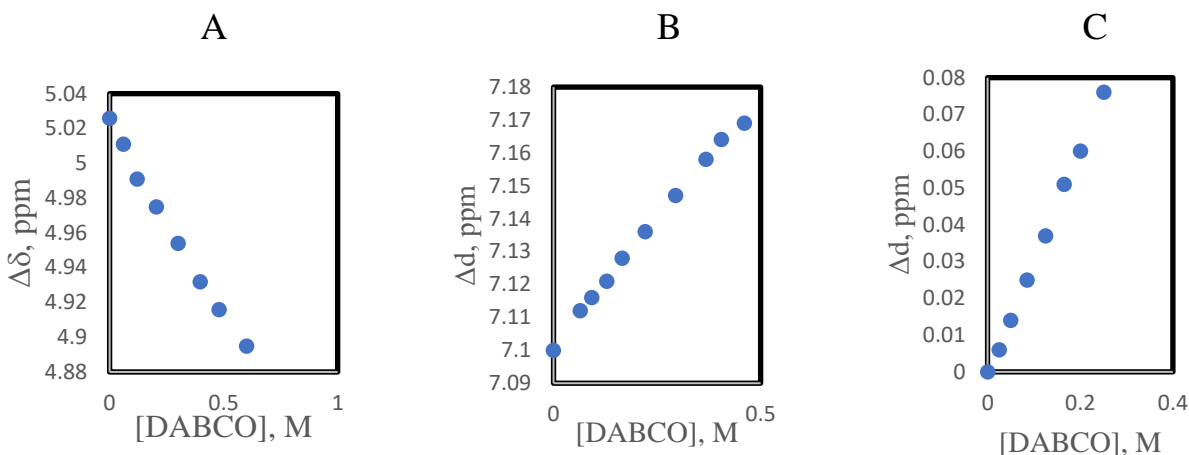


Figure 3-5. ¹H NMR shifts occurring upon the addition of DABCO to solutions containing CHI₃ (A), CHBr₃ (B), and CHCl₃ (C).

However, the addition of TMPD to any of the haloforms under study produced a shift to lower ppm values, indicating increased shielding of this proton (Figure 3-6). NMR measurements of the interactions of haloforms with other aliphatic and aromatic amines confirmed the trends observed with DABCO and TMPD. Specifically, the addition of triethylamine to CHI₃ resulted in a shift of the proton signal to a lower ppm, and similar experiments with CHBr₃ or CHCl₃ resulted in a shift in the opposite direction. On the other hand, the titrations of any of the haloforms with aromatic amines led to shifts in the proton signals to lower ppm values (Figure S8-S12 in the Supporting Information).

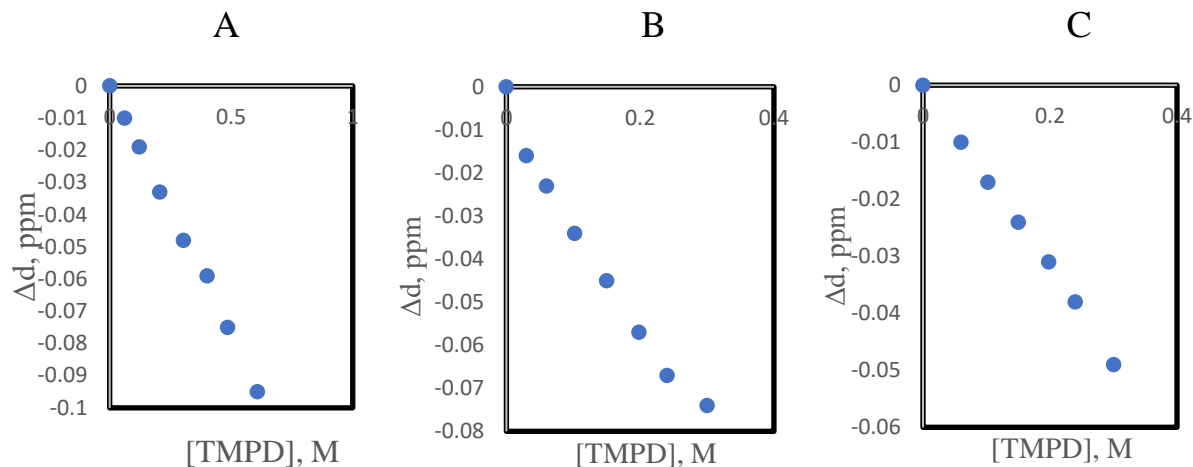


Figure 3-6. ^1H NMR shifts occurring upon addition of TMPD to solutions containing CHI_3 (A), CHBr_3 (B), and CHCl_3 (C).

Similar trends were observed for both UV-Vis and NMR shifts involving the complexes of iodoform, bromoform, and chloroform for other aliphatic and aromatic amines considered in this work (Figure S8-S12 in the Supporting Information).

UV-Vis and NMR measurements showed that both HaB and HyB complexes formed in solutions. However, to obtain the equilibrium constants of these complexes, we needed to determine the spectral characteristics of the complexes by simultaneously analyzing our UV-Vis and NMR spectra. The method considered in the previous work mentioned above by Green and Bertran assumed that only one type of bonding occurs in the solution, even though both types of bonding have been proven to occur.

3.4 Computational Data

To clarify the results of the UV-Vis and NMR measurements, we performed computational analysis of the HaB and HyB complexes of haloforms with amines. DFT calculations were performed using the M062x/def2tzvpp method to optimize the complexes, and interesting results were obtained. The energy and zero-point energies were calculated and the differences in the ΔE

values of the complexes of these aromatic and aliphatic amines with either bromoform or chloroform were small. The HyB complexes of iodoform with amines were also slightly stronger than those of bromoform and chloroform, and all energies were within a range of -5 ± 1 kcal/mol.

The differences in the ΔE was evaluated with this equation; $\Delta E = E_{\text{comp}} - (E_{\text{CHX}_3} + E_{\text{D}}) + \text{BSSE}$, where E_{comp} , E_{CHX_3} , and E_{A} are the sums of the electronic and ZPE of the complex, CHX_3 , and amine, respectively, and BSSE is the basis set superposition error. The energies of the HaB and HyB complexes of CHX_3 with amines, and the energies of the individual molecules and their ZPE values in hartrees are shown in Table S1-S2 in the Supporting Information. Table 3-1 below shows the difference in the calculated energy.

Table 3-1. Energies of HaB and HyB complexes between haloforms and amines resulting from M06-2X/def-TZVPP computations

Amines	ΔE , kcal/mol ^a					
	CHI_3		CHBr_3		CHCl_3	
	HaB	HyB	HaB	HyB	HaB	HyB
DABCO	-7.0	-4.7	-3.5	-4.4	-1.8	-4.0
TMPD	-5.5	-5.5	-3.3	-4.7	-1.9	-4.2
DMA	-5.2	-5.6	-3.8	-4.9	-2.9	-4.8
DMAF	-5.1	-5.2	-3.8	-4.8	-2.9	-4.3
DMACN	-3.9	-4.7	-3.1	-4.3	-2.5	-4.2
p-MeODMA	-4.6	-5.4	-4.1	-5.6	-2.5	-4.2
DMABr	-4.9	-5.2	-3.5	-5.2	-2.8	-4.8
m-MeODMA	-5.1	-6.1	-	-	-2.9	-5.0

As shown in the table 3-2 below, the haloforms and amines were optimized to a near-linear (180°) angle for both HyB and HaB complexes. However, some of these complex angles deviate from this pattern, as shown in the pictures below. While the HaB angles were still nearly linear, the HyB varied significantly. Table 3-2 below illustrates the optimized structures of the haloforms with amine complexes.

Table 3-2: Optimized structures of the calculated complexes with amines, where HaB shows a linear bond angle and HyB shows a deviation from the linear bond angle.

Amines	CHI ₃		CHBr ₃		CHCl ₃	
	HyB	HaB	HyB	HaB	HyB	HaB
DABCO						
DMA						
DMAF						
TMPD						
DMACN						
pMeODMA						
DMABr						
mMeODMA						
TEA						

Table 3-3 below illustrates the distances and angles between the interacting atoms of the complexes.

Table 3-3: Interatomic distances and angles in the HaB and HyB complexes

Amines	HaB		HyB	
	d_{X-N} , Å	Angle, deg	d_{H-N} , Å	Angle, deg
CHI ₃				
DABCO	2.69	179.4	2.05	163.0
TMPD	2.85	178.6	2.16	157.9
DMA	2.96	178.6	2.39	175.2
DMAF	2.90	178.0	2.18	162.9
DMACN	3.07	177.9	2.41	170.8
pMeODMA	3.79	147.8	2.42	159.6
DMABr	2.98	178.9	2.36	163.2
mMeODMA	2.96	178.9	2.34	148.5
TEA	2.79	176.1	2.01	172.2
CHBr ₃				
DABCO	2.80	178.1	2.04	160.7
TMPD	2.87	179.3	2.10	163.1
DMA	2.95	178.2	2.27	174.8
DMAF	2.94	178.4	2.19	158.6
DMACN	3.04	177.8	2.41	174.5
pMeODMA	2.92	178.6	2.25	172.9
DMABr	2.97	178.4	2.52	141.9
mMeODMA	2.96	178.4	2.30	174.1
TEA	2.87	175.0	2.01	165.2
CHCl ₃				
DABCO	2.93	172.4	2.10	153.5
TMPD	2.89	177.8	2.18	159.1
DMA	2.95	176.7	2.46	140.8
DMAF	2.93	178.9	2.23	154.9
DMACN	3.03	175.6	2.67	133.6
pMeODMA	2.90	176.5	2.42	141.7
DMABr	2.96	177.7	2.54	137.3
mMeODMA	2.95	179.2	2.34	164.5
TEA	2.93	174.0	2.06	159.8

Complexes of haloforms with aliphatic and aromatic amines produced energy minima, indicating I...N or H...N bonding. This interaction was somewhat stronger for the haloforms in HaB complexes with aliphatic amines, such as DABCO, than for most aromatic amines. These computational results agree with the experimental X-ray structural data, that is, a shorter I...N separation in solid-state complexes of CHI₃ with DABCO compared to those in association with

aromatic amines and shorter I...N distances in the iodoform complex with DABCO than with Br...N distances and similar associations with CHBr_3 and CHCl_3 .

TD DFT calculations showed that the UV-Vis spectra of all HaB complexes contained absorption bands (Table 3-4) which were red-shifted and substantially more intense than the absorption bands of the individual compounds. These bands are related to transitions involving orbitals localized on both haloforms and amines. In contrast, the UV-Vis spectra of the optimized HaB complexes were very close to that of the superposition of individual components. These results are consistent with the reported data and indicate that the appearance of new absorption bands in the UV-Vis range is related to the formation of HaB complexes.

The proton signals of the haloforms in the NMR spectra of the optimized HaB complexes were shifted to lower ppm values, indicating increased shielding of these protons. In the case of all HyB associations, the signals shifted to higher ppm values. These results agree with earlier observations of opposite shifts in the proton signals of haloforms related to halogen and hydrogen bonding. However, even though calculations (and data on similar associations) suggest that CHBr_3 and CHCl_3 form stronger HyB complexes with aromatic amines, experimental measurements showed a uniform shift of the haloform proton signal to lower ppm values upon the addition of this amine to any of the haloforms, as shown in the earlier figures.

Table 3-4: Calculated UV-Vis and NMR characteristics of the HaB and HyB complexes

CHX ₃	D	HaB complexes			HyB complexes		
		λ_{\max} , nm	$\epsilon \times 10^{-3}$, M ⁻¹ c m ⁻¹	$\Delta\delta$, ppm	λ_{\max} , nm	$\epsilon \times 10^{-3}$, M ⁻¹ c m ⁻¹	$\Delta\delta$, ppm
CHI ₃	DABCO	311	9.0	-1.539	302	1.4	1.847
	TMPD	335	7.2	-0.669	295	4.5	1.506
	DMA	312	3.2	-0.614	263	3.2	-0.729
	DMAF	308	10.0	-0.521	229	7.0	1.241
	DMACN	258	28.0	-0.491	263	26	-0.866
	pMeODMA	370	3.8	-0.456	286	4.4	-1.270
	DMABr	312	8.5	-0.457	242	15.0	0.007
	mMeODMA	318	7.5	-0.442	261	4.7	-0.413
CHBr ₃	DABCO	259	7.5	-0.452	212	2.8	2.502
	TMPD	285	8.0	-0.437	245	20.0	1.503
	DMA	270	6.0	0.030	230	14.0	0.283
	DMAF	270	7.0	-0.446	229	10.0	1.150
	DMACN	267	30.0	-0.397	262	27.0	-0.666
	pMeODMA	284	16.0	-0.360	231	16.0	0.397
	DMABr	272	7.0	-0.343	240	19.0	-0.690
	mMeODMA	275	6.0	-0.312	231	11.0	0.247
CHCl ₃	DABCO	216	3.3	-0.230	220	25.0	2.119
	TMPD	290	3.0	-0.344	247	20.1	1.353
	DMA	235	14.0	-0.340	259	3.8	-0.386
	DMAF	274	3.0	-0.442	263	2.2	1.030
	DMACN	263	30.0	-0.332	263	27.0	-0.952
	pMeODMA	236	18.0	-0.260	278	2.8	-0.280
	DMABr	274	2.5	-0.329	273	3.0	-0.723
	mMeODMA	257	7.0	-0.249	238	9.5	0.113

- a. λ , in nm, (ϵ) for individual compounds are CHI₃ – 304 (3050), CHBr₃ -223 (2500), CHCl₃ 175 (1600), δ (in ppm) for CHI₃ – 7.0287, CHBr₃ – 7.6825, CHCl₃ – 7.582.

The surface electrostatic potentials of the various haloforms and amines are shown in Figure 3-7.

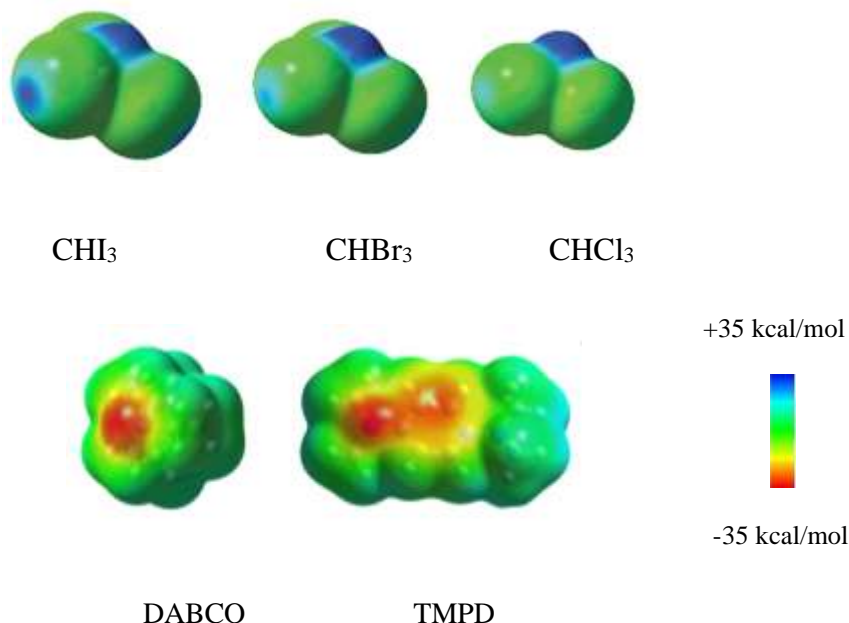


Figure 3-7. Electrostatic potential (calculated at 0.001 electrons Bohr⁻³ electronic density) on the molecular surfaces of CHI_3 , CHBr_3 , CHCl_3 , DABCO, and TMPD.

Theoretical studies have shown that polarization plays an important role in this process. The locations of V_{\min} on the surfaces of nitrogen atoms in aliphatic and aromatic amines suggest that they are attracted to (-holes on the surface of either hydrogen or halogen atoms in haloforms. The blue areas represent the positive potentials on the surface for both hydrogens (top) and halogens (side). Due to the shift of electron density toward the electron-withdrawing group, an area of partial positive charge, known as the σ -hole, is formed opposite to the covalent bond (blue area in Figure 3-7). HaB acceptor species "fill" the σ -hole by coordinating its negative charge with the HaB donor species.

Analysis of the potential energy landscape revealed the presence of additional minima for the complexes of haloforms with TMPD and other aromatic amines. The interactions between the halogen bond donor and acceptor were highly directional. This led to the conclusion that these

interactions were electrostatic, and that the areas of more positive potential attracted areas of negative potential in the conjugated molecule. For other aromatic amines, aside TMPD, the negative potential also extends from the surface of the nitrogen atom to the aromatic ring (Figure S13 in the Supplementary Information).

To clarify the reasons for the variations in the interaction energies, we compared their values with changes in the maximum (V_{\max}) and minimum (V_{\min}) electrostatic potentials on the surfaces of haloforms and amines, respectively (Table 3-5). The dependence of the ΔE values on the difference $V_{\max} - V_{\min}$ (found for the individual haloforms and amines).

Table 3-5. V_{\max} values on the surfaces of halogen (V_{\max}^X) and hydrogen (V_{\max}^H) atoms (at 0.001 a.u. electron density) in the individual haloforms and the molecules polarized by the presence of electron-rich centers near halogen (in the HaB complex) or hydrogen (in the HyB complex) atoms.

Molecule	V_{\max}^H , a.u.	V_{\max}^X , a.u.
CHI ₃ (Ind)	0.0541	0.0425
CHI ₃ (HaB complex)	0.0434	0.124
CHI ₃ (HyB complex)	0.108	0.0334
CHBr ₃ (Ind)	0.0611	0.0302
CHBr ₃ (HaB complex)	0.0528	0.0828
CHBr ₃ (HyB complex)	0.108	0.0181
CHCl ₃ (Ind)	0.0624	0.02
CHCl ₃ (HaB complex)	0.055	0.055
CHCl ₃ (HyB complex)	0.103	0.0141

For the HaB complexes, the increase in the difference in potentials was accompanied by an increase in the magnitude of the (negative) ΔE values. However, for the HyB complexes, no such correlation was observed. Furthermore, while the V_{\max} values on the surfaces of hydrogen atoms are higher than those on the surfaces of halogen atoms in all individual haloforms (which is reflected in the $V_{\max} - V_{\min}$ differences), halogen bonding is the dominant mode of interaction of the iodoform (Figure 3-8).

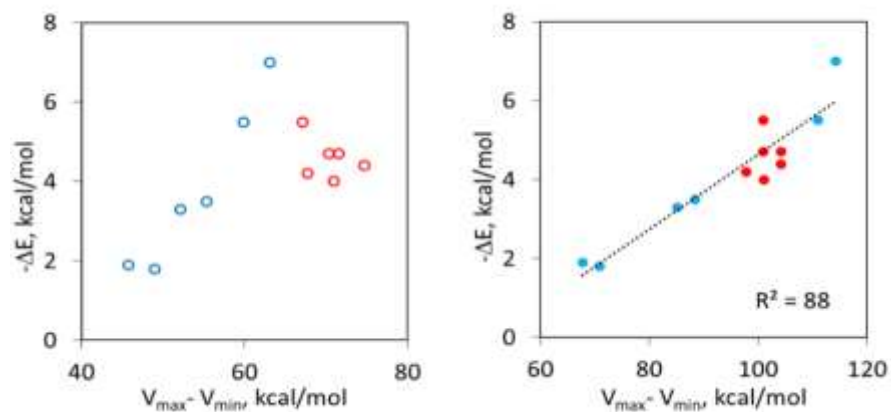


Figure 3-8. Correlations between the interaction energies in the HaB and HyB complexes (blue and red circles, respectively) with DABCO and TMPD and the electrostatic potentials difference on the surfaces of interacting atoms in the individual (left) and polarized molecules (right).

In addition, calculations of complexes with TMPD produced minima in which hydrogen or halogen substituents of haloforms were directed toward carbon atoms in the aromatic ring or middle of C-N bonds, *vide infra*).

The quantum Theory of Atoms in Molecules (QTAIM) analysis of the optimized structures showed bond paths (orange lines in Figure 3-9) from nitrogen atoms to halogen or hydrogen substituents of haloforms in the HaB and HyB complexes, respectively. It also reveals the (3,-1) Bond Critical Points (BCPs) along these bond paths (small orange spheres). Bonding interactions between nucleophilic nitrogen atoms and haloform halogens or hydrogen were further confirmed by non-covalent index (NCI) analysis. The NCI treatment showed the presence of blue-colored discs located at the BCPs between the nitrogen atoms of amines and halogen or hydrogen atoms of haloforms, which indicates a moderately strong intermolecular attraction between these atoms. In addition to the bond paths and BCPs between the nitrogen atoms and hydrogens, HyB complexes showed bond paths and BCPs between halogen atoms of haloforms and hydrogen substituents or aromatic carbons of amines. The NCI analysis showed green surfaces corresponding to

nonbonding or very weak bonding interactions along these bond paths. This indicates that they represent secondary interactions that are most likely supported by the close approach of the haloform to amines.

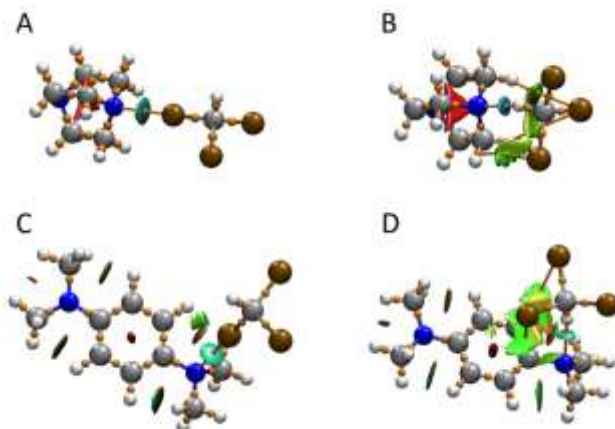


Figure 3-9. Superposition of the results of the QTAIM and NCI analyses on the structures of the HaB complexes of CHBr_3 with DABCO (A) and TMPD (C) and HyB complexes with DABCO (B) and TMPD (D). The bond paths and critical (3, -1) points (from QTAIM) are shown as orange lines and spheres, respectively, and the blue-green discs indicate areas of bonding interactions (from NCI).

The characteristics of the BCPs on the HaB and HyB bond paths obtained from QTAIM analysis corroborate the similarities of these associations between amines and haloforms. The electron densities and energies of the BCPs are presented in Table 3-6, and that of other haloforms complexes with amines are shown in Table S3 in the Supporting Information.

Table 3-6. Electron densities and energies ($\rho(r)$ and $H(r)$, in a.u.) at BCPs along HaB and HyB bond paths.

CHX ₃	D	HaB complexes		HyB complexes	
		$\rho(r) \times 10^2$	$H(r) \times 10^3$	$\rho(r) \times 10^2$	$H(r) \times 10^3$
CHI ₃	DABCO	3.65	-3.70	2.76	-1.11
	TMPD	2.70	-1.11	2.15	0.44
CHBr ₃	DABCO	2.39	0.51	2.81	-1.31
	TMPD	2.07	0.76	2.16	0.34
CHCl ₃	DABCO	1.52	1.61	2.53	-0.37
	TMPD	1.66	1.51	2.05	0.57

However, it should be noted that in contrast to the singular solid-state donor/acceptor arrangement, solution-phase complexes are subject to fluctuations around the optimized minimum (or several local minima), which might affect the spectral characteristics. Indeed, analysis of the potential energy landscape shows that the HaB and HyB complexes between CHX_3 and aromatic amines are characterized by shallow minima. The variations of the X...N or H...N separations by about 0.5 Å are accompanied by energy changes of less than 1 kcal/mol (Figure 3-10).

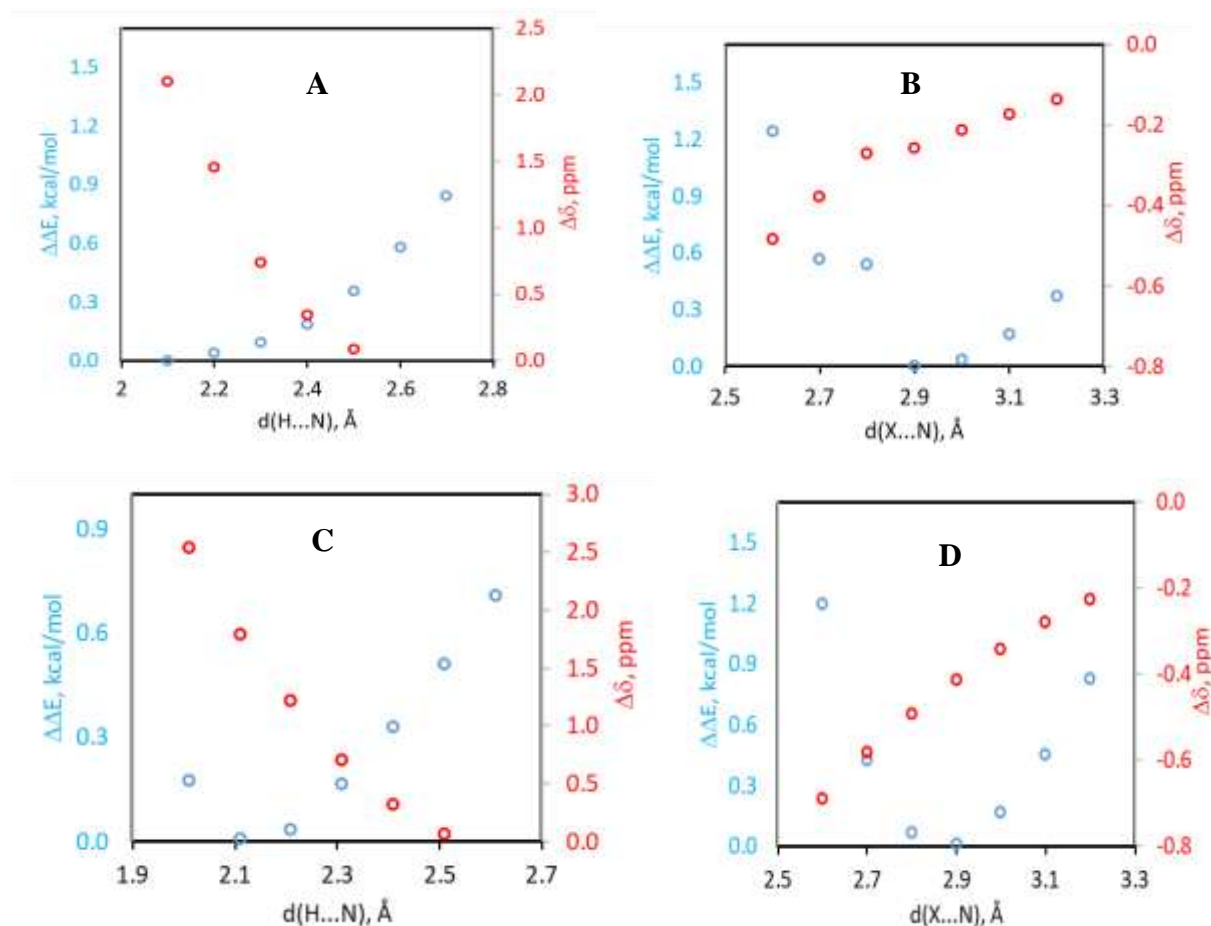


Figure 3-10. Effect of variations in interatomic H...N and X...N separations on the energies of HyB and HaB complexes (blue circle) relative to that of the energy minimum and the shift of the proton signal in their NMR spectra (red circles) relative to that in the individual CHX_3 for: A) HyB complexes of CHCl_3 with DABCO, B) HaB complexes of CHCl_3 with DABCO, C) HyB complexes of CHBr_3 with TMPD, and D) HaB complexes of CHBr_3 with TMPD.

Changes in the NMR spectra accompanied these structural variations, that is, the increase in the separation was accompanied by a decrease in the difference in the position of the signal in the complex compared to that of the individual haloform. While shallow minima imply the co-existence of assemblies of associations with varying separations, the average distances and NMR shifts for these assemblies seem close to those found for the minima. As such, they do not substantially affect the general trends of the NMR shifts. However, analysis of the potential energy landscape also revealed the presence of additional minima for the complexes of haloforms with TMPD. The structural overlap (Figure 3-11) demonstrates that the alternative HyB structures were similar. The main structural difference was the shift in the position of the protons in the alternative structures from the nitrogen atom toward the aromatic ring; therefore, it was directed toward the middle of the C-N bond or the aromatic carbon in the ortho-position of the amino group. Computational analysis also revealed the presence of HaB complexes with TMPD, in which the halogen atom was directed toward aromatic carbons. Specifically, in the alternative structure of CHI_3 with this molecule, the iodine substituent of the iodoform is directed toward a nitrogen-bonded carbon atom. The Figure 3-11 illustrate the structural variation in the complexes of haloforms (CHI_3 , CHBr_3 , and CHCl_3) with TMPD.



Figure 3-11. Structural overlap of the complexes of TMPD with CHI_3 (left), CHBr_3 (middle), and CHCl_3 (right) formed via $\text{H}\cdots\text{N}$ bonding and alternative complexes (shown as red structures).

3.5 Simultaneous Treatment of the Experimental UV-Vis and NMR Data

Using the values of the NMR shifts obtained from the calculations, the experimental, NMR, and UV-Vis spectra were fitted to Equations 24 and 25 (Experimental section), which describe the changes in these characteristics with the addition of DABCO, TMPD, and other amines to solutions of haloform molecules. This fitting was performed using Origin 2016. In the fitting procedure, both the NMR shifts and UV-Vis absorption intensities were plotted against increasing amine concentrations with a constant concentration of haloforms. These values were then fitted simultaneously by Origin to Equations 24 and 25 using the values of the formation constants of the hydrogen and halogen-bonded complexes as adjustable parameters. An example of such a fitting is shown in Figure 3-12. Similar diagrams were generated for other amines (Figure S14 Supporting Information).

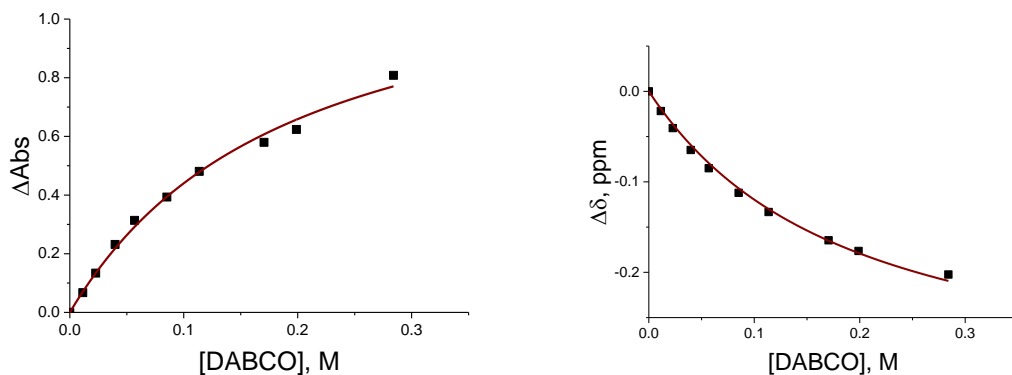


Figure 3-12. Dependencies of ΔAbs and $\Delta\delta$ values in solutions with constant concentration of CHI_3 (0.01 M) and variable concentrations of DABCO. Solid lines show the simultaneous multivariable fitting of the UV-Vis and NMR titrations data

This figure above shows the fitting (using Origin 16) of the UV-Vis spectral data of the solutions containing constant concentrations of CHI_3 and variable concentrations of aliphatic and aromatic amines to 1:1 binding isotherm as $\Delta\text{Abs} = \epsilon l \times C_{\text{com}} = \epsilon l \times \left\{ (C_{\text{A}}^0 + C_{\text{D}}^0 + 1/K_{\text{eff}}) - \left((C_{\text{A}}^0 + C_{\text{D}}^0 + 1/K_{\text{eff}})^2 - \right. \right.$

$4C_A^0C_D^0)^{0.5}\}/2$, where ΔAbs is the absorbance of the complex at a specific wavelength (obtained by subtraction of the absorption of the components from the spectra of the mixtures), C_{com} is the concentration of the complex, and C_D^0 and C_A^0 are initial concentrations of CHX_3 and amine, ϵ and l are extinction coefficient of the complex and the length of the cell which was used in the UV-Vis measurements. K_{eff} is the effective formation constant of the complex.

The K_{HaB} and K_{HyB} values were obtained by simultaneous nonlinear fitting using multiple variable options with the Levenberg-Marquardt iteration algorithm in OriginPro. Table 3-7 shows the formation constants for the HaB and HyB complexes formed between two haloform compounds (CHBr_3 and CHI_3) with DABCO and TMPD. The formation constants represent the strength of the complexes formed between the haloform compounds and the amines. Higher values indicate stronger interactions and more stable complexes as seen in the case of the iodoform complexes with DABCO and TMPD. The uncertainties (\pm) indicate the margin of error in the experimental measurements.

Table 3-7. Formation constants of HaB and HyB Complexes of CHI_3 and CHBr_3 with DABCO and TMPD complexes.

	CHBr₃		CHI₃	
Amines	K_{HaB}, M⁻¹	K_{HyB}, M⁻¹	K_{HaB}, M⁻¹	K_{HyB}, M⁻¹
DABCO	0.27±0.03	0.12±0.01	3.7±0.3	2.0±0.2
TMPD	-	-	0.3±0.1	0.3±0.1

CHAPTER 4. HALOGEN AND HYDROGEN BONDING BETWEEN (HALO)IMIDAZOLIUM CATIONS AND HALIDES

The differences between the HaB and HyB interactions between haloforms and amines were studied in the first part of this work. To further differentiate HaB from HyB, we studied halogen- and hydrogen-bonded complexes in a solution of (halo)imidazolium and halides. We changed both the halogen bond donors and acceptors. However, there was no competition between HaB and HyB in this case because the (halo)imidazolium cations contained either halogen or hydrogen substituents.

In the case of (halo)imidazolium cations connected via halogens or hydrogen to halides, HaB, and HyB interactions were compared and contrasted. In this study, HaB refers to the interaction between a halogen atom on the (halo)imidazolium cation and a halide anion, whereas hydrogen bonding involves the interaction between a hydrogen atom on the (halo)imidazolium cation and a halide anion. X-ray structural analysis has been investigated by some research groups in the past, and it shows the structural differences and provides a detailed understanding of the HaB and HyB interactions between (halo)imidazolium salts and halides.

Based on previous work, X-ray crystal structures provide a visual representation of the hydrogen bonding interactions between imidazolium cations and halide anions. This is shown in figure 1.2 and 1.5.

4.1 UV-Vis Measurement of HaB and HyB Complex in Solution.

UV-Vis measurements were performed to determine the formation of complexes in solution. The addition of the H-Im-iPrArI electrophile to solutions of TBAI in dichloromethane resulted in new absorption bands at ~290 nm and ~ 265 nm, which were not present in the spectra of the separate

components. The increasing absorption bands indicated that halogen bonding occurred in the solution. This suggested substantial molecular orbital interactions in HaB. The spectra are shown in Figure 4-1.

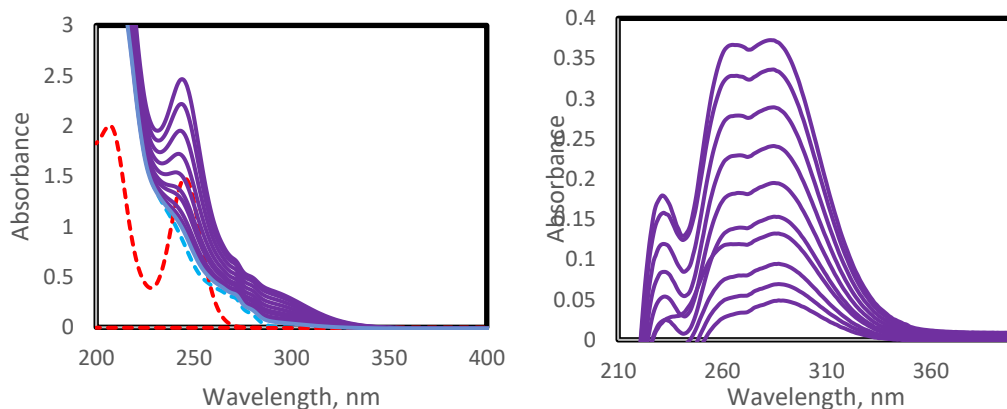


Figure 4-1. (Left) Spectra of solutions with constant concentrations of H-Im-iPrArI (0.4mM) and various concentrations of tetrabutylammonium iodide (TBAI). The spectra of the solutions of the individual reactants are shown by dashed blue (H-Im-iPrArI) and red (TBAI) lines. (Right) Spectra of the complexes obtained by subtracting the absorption of components from the spectra of their mixtures.

Regression analysis was performed by fitting the UV-Vis data considering the absorbance points at 290 and 265 nm, and the two diagrams shown in Figure 4-2 were obtained.

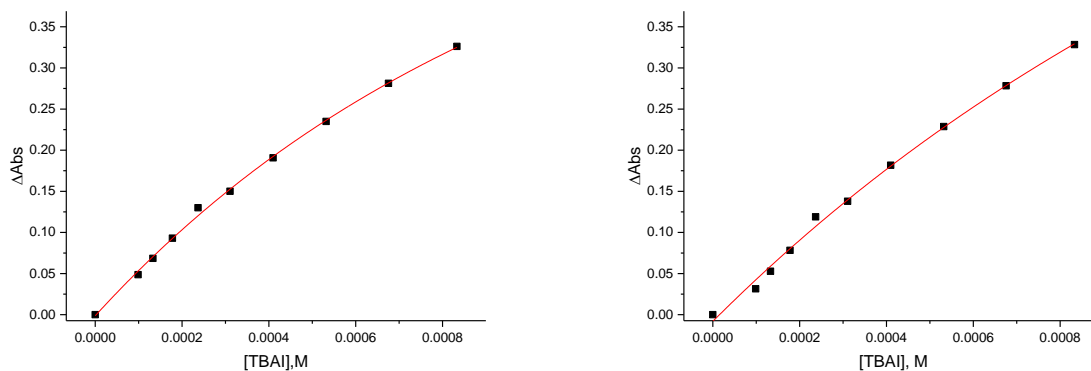


Figure 4-2. Dependencies of Abs values in solutions with constant concentrations of H-Im-iPrArI (0.4mM) and variable TBAI concentrations. The solid lines show the fitting of the UV-Vis titration data.

A similar interaction between H-Im-iPrArI and TBABr in dichloromethane resulted in a new absorption band at ~ 235 nm, which was not present in the spectra of the separate components. The increasing absorption bands indicated that halogen bonding occurred in the solution and it is shown in the Figure 4-3 below.

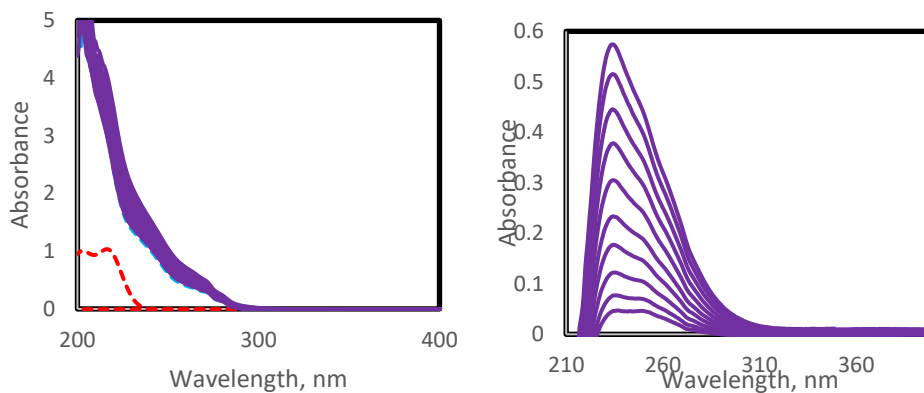


Figure 4-3. (Left) Spectra of solutions with constant concentrations of H-Im-iPrArI (0.4mM) and various concentrations of tetrabutylammonium bromide (TBABr). The spectra of the solutions of the individual reactants are shown by dashed blue (H-Im-iPrArI) and red (TBABr) lines. (Right) Spectra of the complexes obtained by subtracting the absorption of components from the spectra of their mixtures.

A similar fitting was performed considering the absorbance points at a wavelength of 235 nm, and Figure 4-4 was obtained.

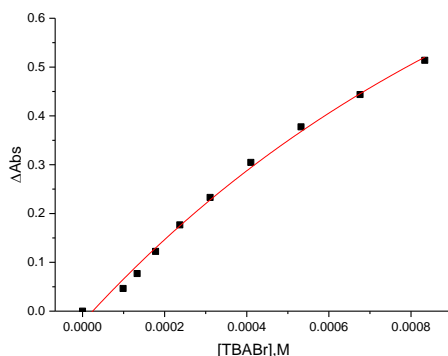


Figure 4-4. Dependencies of the Δ Abs values in the solutions with a constant concentration of H-Im-iPrArI (0.4mM) and variable TBABr concentrations. The solid lines show the fitting of the UV-Vis titration data.

The addition of the H-Im-iPrArI electrophile to solutions of TBACl in dichloromethane did not result in the formation of a new absorption band after subtracting the spectra of the separate molecules. The results are shown in Figure S15 in the Supporting Information.

As a result of fitting the UV-Vis data of complex formation at specific wavelengths corresponding to the band of the complex, the following formation constants and the coefficient of absorptivity were obtained, as shown in Table 4-1.

Table 4-1: Formation constants, wavelengths and the coefficients of absorptivity of halogen-bonded complexes.

Imidazolium	Halides	Complexes		K, M^{-1}	$\epsilon, M^{-1}cm^{-1} \times 10^2$	λ_{max}, nm	K, M^{-1}	$\epsilon, M^{-1}cm^{-1} \times 10^2$
		λ_{max}, nm	K, M^{-1}					
H-Im-iPrArI	I ⁻	265	413±214	32±9	290	980±208	20.5±2.3	
	Br ⁻	235	676±362	38±10				

The addition of the H-Im-iPrArH electrophile to solutions of TBAI in dichloromethane did not result in the formation of a new absorption band after subtracting the spectra of the separate molecules. This result indicates that there was no HaB complex formation within the system, as the HyB complex could not be observed by UV spectroscopy. This is shown in Figure 4-5.

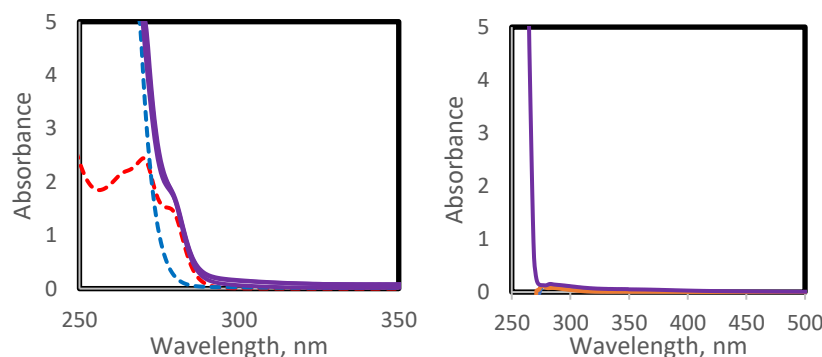


Figure 4-5. (Left) Spectra of solutions with constant concentrations of H-Im-iPrArH (0.4mM) and various concentrations of tetrabutylammonium iodide (TBAI). The spectra of the solutions of the individual reactants are shown by dashed blue (H-Im-iPrArH) and red (TBAI) lines. (Right) Spectra of the complexes obtained by subtracting the absorption of components from the spectra of their mixtures.

Similarly, for the complex formed between H-Im-iPrArH and iodide, the interaction of H-Im-iPrArH with TBABr did not produce a new band for the HyB complex. This further proves that the HyB complex cannot be observed by UV-Vis spectroscopy (Figure S16 Supporting Information).

4.2 ¹H NMR Measurement of HaB and HyB Complex in Solution

To further study the HaB and HyB complexes in solution, ¹H NMR was used to measure complex formation between the (halo)imidazolium and halides. In particular, the HyB association of H-Im-iPrArH with halides led to a shift of their protons to higher ppm (Figure 4-6), and the HaB associations of H-Im-iPrArI with halides led to the opposite shifts of their proton signals (lower ppm) in the NMR spectra, as shown in Figure 4-7 after fitting with origin pro (2016). These results are consistent with those of previous studies, as well as studies in our lab involving the interaction of haloforms with halides and the most recent work, as discussed in chapter three, involving the interaction of haloforms with amines. The HaB complexes shifted to lower ppm (or decreased ppm), while the HyB complexes shifted to higher ppm (or increased ppm).

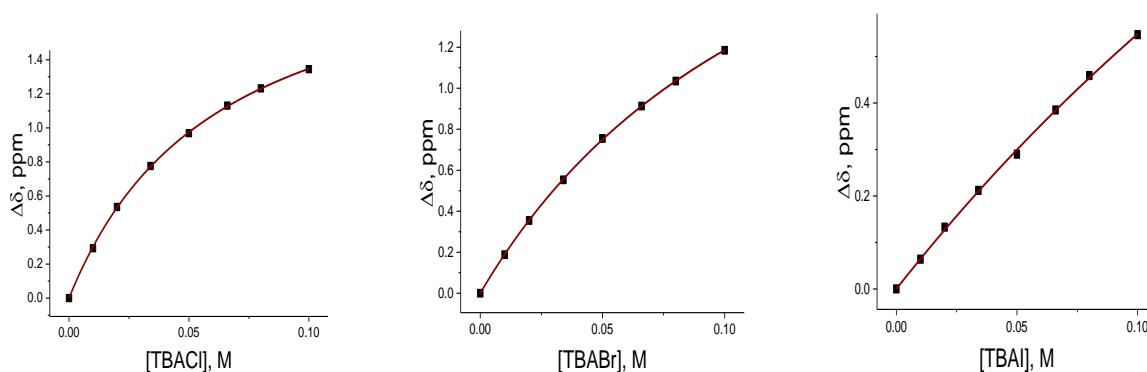


Figure 4-6. The dependencies of the δ values in solutions with a constant concentration of H-Im-iPrArH and variable concentrations of TBACl, TBABr, and TBAI showed stronger HyB interactions in the order Cl⁻>Br⁻>I⁻ and a shift to a positive $\Delta\delta$, ppm.

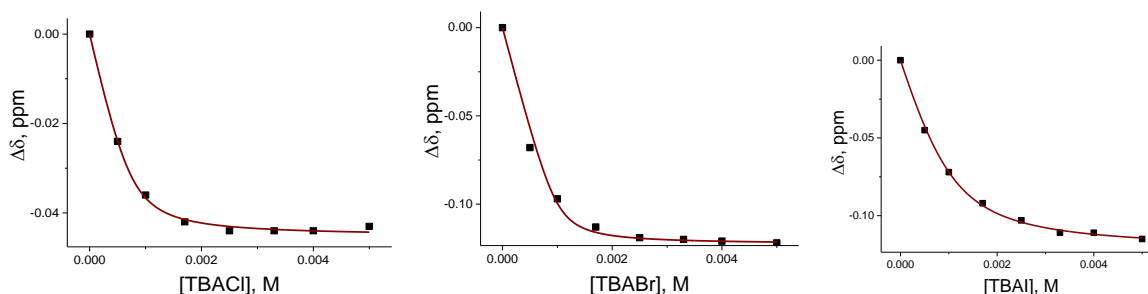


Figure 4-7. The dependencies of the δ values in solutions with a constant concentration of H-Im-iPrArI and variable concentrations of TBACl, TBABr, and TBAI showed stronger HaB interactions in the order of Cl^- , $\text{Br}^- > \text{I}^-$ and a shift to a negative $\Delta\delta$, ppm.

The values for the formation constants and change in chemical shifts were obtained after fitting the NMR data, as shown in Table 4-2

Table 4-2. The K values obtained by the nonlinear fitting algorithm of the NMR data

Imidazolium	Halides	K, M^{-1}	$\Delta\delta\text{c}$
H-ImPrAr-H	Cl^-	16.6 ± 0.3	2.17 ± 0.02
	Br^-	7.3 ± 0.1	2.82 ± 0.03
	I^-	2.1 ± 0.3	3.23 ± 0.46
H-Im-iPrArI	Cl^-	$(12 \pm 2) \times 10^3$	-0.0451 ± 0.0004
	Br^-	$(10 \pm 1) \times 10^3$	-0.125 ± 0.001
	I^-	$(2.8 \pm 0.5) \times 10^3$	-0.035 ± 0.001

K is a measure of the strength of the interaction between the imidazolium cation and the anion, with a larger K indicating a stronger HyB interaction. The values of K obtained in this study range from 2.1 to 16.6 M^{-1} , with the strongest interaction observed for H-ImPrAr-H with Cl^- . The change in chemical shifts ($\Delta\delta\text{c}$) associated with halogen and hydrogen bonded complexes is typically observed as the difference in the chemical shift values of the uncomplexed species and the complex species. It is a measure of the change in electron density around the imidazolium cation upon interaction with the anion. The values of $\Delta\delta\text{c}$ obtained in this study range from 2.17 to 3.23 ppm, with the largest chemical shift change observed for H-ImPrAr-H with I^- . These results suggest that

the strength of the interaction between imidazolium cations and halide anions decreases in the order $\text{Cl}^- > \text{Br}^- > \text{I}^-$.

4.3 Computational Data

The DFT calculations done with M062x/def2tzvpp method to optimize the complexes showed some exciting results (Table 4-3). In addition, TD and NBO calculations were performed.

Table 4-3: Energies and UV-Vis values of HyB and HaB complexes between imidazolium and halides, and NBO charges on the halides, (M06-2X/def-TZVPP computations in acetonitrile).

Complexes	ΔE , kcal	λ_{max} , nm	ϵ , $\text{M}^{-1}\text{cm}^{-1}$	Δq , e
H-ImAr-I---I-	-8.2	238	46000	0.13
H-ImAr-I---Cl-	-11.5	204	30000	0.14
H-ImAr-I---Br-	-9.8	218	44000	0.13
H-ImAr-H---I-	-6.9	229	2500	0.05
H-ImAr-H---Cl-	-9.9	194	20000	0.07
H-ImAr-H---Br-	-8.5	201	4550	0.06
Cl-ImAr-I---I-	-9.3	246	53000	0.17
Cl-ImAr-I---Cl-	-12.9	238	16500	0.17
Cl-ImAr-I---Br-	-10.9	225	40000	0.16

The table shows that the HaB and HyB complexes of chloride are generally more stable than those of bromide and iodide because they have the most negative energy difference. The λ_{max} and ϵ values indicate the absorption spectra of the complexes in the UV-Vis range. The complexes generally exhibited strong absorption in the range of 200-250 nm. The energies of the HaB and HyB complexes of (halo)imidazolium cations with halides, and the energies of the individual molecules and their ZPE values are shown in Table S4 in the Supporting Information.

The NBO charges on the halides show variations depending on the specific complex and the halide involved. The halogen bonded complexes have higher charge Δq than the hydrogen bonded complexes. These charges reflect the redistribution of electron density resulting from the interactions within the complexes.

The EDA method was used to analyze the interaction between the two molecules, decomposing the total interaction energy into different components. The Pauli repulsion, electrostatic interactions, orbital interactions, and dispersion components are illustrated in the Figure 4-8.

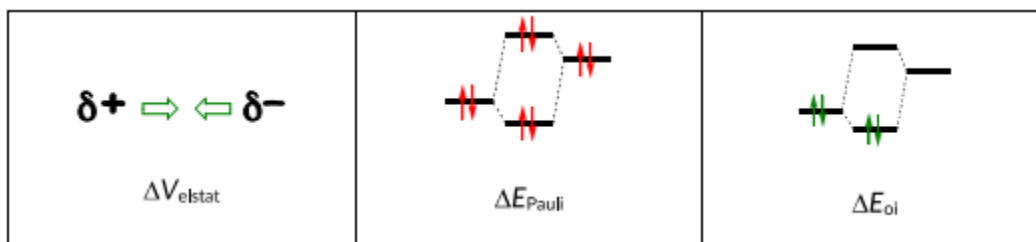


Figure 4-8. Molecular orbital interaction diagrams

The different EDA components are as follows:

- Pauli repulsion: repulsion due to overlapping electron clouds between two molecules.
- ES (Electrostatic): Coulombic attraction or repulsion between two molecules.
- MO (orbital interaction): interaction between the occupied and unoccupied molecular orbitals of two molecules.
- Disp (dispersion): Attractive interactions owing to fluctuations in the electron density of the two molecules.

EDA analysis was performed with the software for chemistry and materials: Amsterdam modeling suites using the functional B3LYPD3(BJ) functional. Table 4-4 illustrates the values of various EDA components obtained after computation. This table provides a quantitative understanding of the different contributions to the interactions between (halo)imidazolium and halides. Therefore, in general, the high values of the HaB interactions in the table for most of the parameters suggest that there is a significant amount of interactions between the (halo)imidazolium and halide molecules than for HyB.

Table 4-4 Contribution of different components to interaction energies between imidazolium cations and halides (from EDA) and charge transfer (Δq) in the corresponding complexes values between (halo)imidazolium and halides

Complexes	Pauli, kJ/mol	ES, kJ/mol	MO, kJ/mol	Disp, kJ/mol	Δq, e
H-ImAr-I---Cl-	147.1	-358.4	-162.4	-10.0	0.25
H-ImAr-I---Br-	129.5	-333.4	-143.6	-11.4	0.23
H-ImAr-I---I-	123.1	-313.9	-130.9	-13.9	0.24
H-ImAr-H---Cl-	75.5	-327.7	-103.5	-18.1	0.12
H-ImAr-H---Br-	71.1	-310.6	-90.7	-21.6	0.10
H-ImAr-H---I-	72.1	-294.9	-77.5	-26.5	0.09
Cl-ImAr-I---Cl-	181.6	-386.9	-187.2	-10.4	0.27
Cl-ImAr-I---Br-	159.9	-359.0	-166.5	-12.0	0.26
Cl-ImAr-I---I-	154.2	-339.0	-154.3	-14.6	0.27

The MO components for the halogen bonding complexes range from -162.4kJ/mol to -187.2kJ/mol, while those for the HyB complexes range from -77.5kJ/mol to -103.5kJ/mol which are three times lesser than the values of HaB. This suggest that molecular orbital interactions contribute significantly to HaB than for HyB. Similar trends to MO components are seen in the case of ES and Pauli. While the contribution in terms of dispersion is higher for HyB than for HaB which as nearly comparable.

The Hirschfeld charge transfer (Δq) values given in the table involving halogen and hydrogen bonding complexes are a measure of the electron transfer between the atoms involved in the bonding interaction. These values provide an estimate of the strength of the HaB and HyB interactions. Larger Hirschfeld charge transfer values indicate stronger interactions, while smaller values indicate weaker interactions. In the given table, the Hirschfeld charge transfer values for both HaB and HyB interactions are relatively large, ranging from 0.09 to 0.27, suggesting that the interactions are strong in generally. But it is stronger in this case for HaB than HyB due to the higher charge transfer values of HaB than for HyB. The values for the same halogen atom in different complexes are similar.

CHAPTER 5. ELECTRON TRANSFER REACTION BETWEEN IODINE WITH AMINES AND SOME HETEROCYCLIC COMPOUNDS

We have also worked on another interesting area that involves the study of halogen-bonded complexes between molecular iodine with amines and some nitrogen-containing heterocyclic compounds. A fascinating aspect of halogen bonding is its ability to facilitate electron transfer (ET) between halogens and electron-rich compounds. In the case of molecular iodine (I_2), it can undergo ET reactions with amines and nitrogen-containing heterocyclic compounds. These reactions are typically initiated by the formation of a halogen bond between the iodine atom and nucleophile, which results in an iodine-nucleophile complex.

This complex can then undergo a one-electron transfer process in which the nucleophile donates an electron to the iodine atom, resulting in the formation of a radical cation, and triiodide ion.

5.1 X-ray Crystallographic Analysis

In this study, we attempted to obtain a complex by interacting iodine with various amines and heterocyclic compounds. Unfortunately, most of the crystals preparation was not successful except for two which X-ray crystallography results showed the structures of the redox products formed from the interaction of iodine with MPTZ and pMeODMA. The crystals were grown and analyzed, as discussed in the experimental section. The crystal structures obtained from this preparation are shown in Figure 5-1.

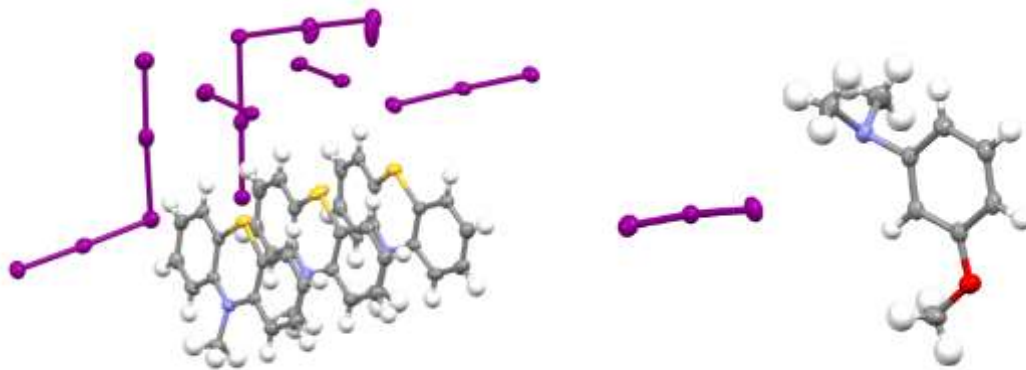


Figure 5-1. X-ray structures showing the formation of redox products from the interaction of I_2 and MPTZ (left), I_2 , and pMeODMA (right).

The interaction of iodine with 10-methylphenothiazine dissolved in dichloromethane led to the formation of redox products, such as triiodide, iodine, and pentaiodide, with the cation radical of MPTZ, while the interaction of iodine with pMeODMA in dichloromethane also led to the formation of triiodide and the cation radical of pMeODMA respectively.

5.2. UV-Vis Measurement of HaB Complex in Solution.

UV-Vis's measurements demonstrated HaB complexes formation for most of the complexes studied in dichloromethane. This is because band formation still occurred when the absorption of amines, iodine, and the baseline were subtracted. Typical results of UV-Vis measurements of the solution series with a constant concentration of iodine and various concentrations of amines are shown in Figure 5-2.

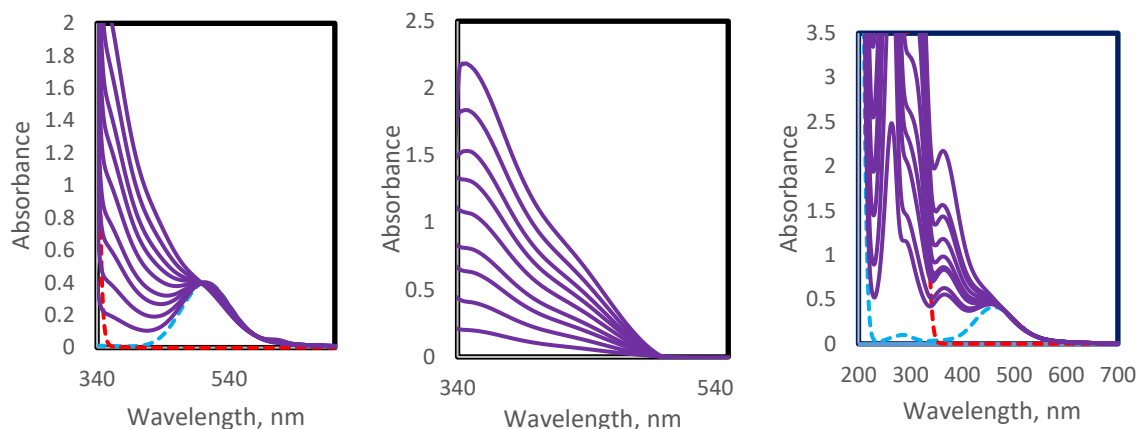


Figure 5-2. (Left) Spectra of solutions with constant concentrations of I_2 and various concentrations of DMABr in DCM. The Spectra of the solutions of the individual reactants are shown as dashed blue (I_2) or red (DMABr) lines. (Center) Spectra of the complexes obtained by subtracting the absorption of components from the spectra of their mixtures in DCM. (Right) Spectra of the solutions with constant concentrations of I_2 and various concentrations of DMABr in AN.

The addition of I_2 electrophiles to solutions of DMABr in dichloromethane resulted in a new absorption band at ~ 356 nm (left and center), which was not present in the spectra of the separate components. This band was persistent and its intensity increased with increasing amine concentration at a constant concentration of I_2 . The UV result involving the interaction of I_2 with DMABr in acetonitrile (right) indicated the formation of triiodide (I_3^-) species. This can be seen from the appearance of an absorption band around 360 nm in the UV spectrum of the reaction mixture. However, the reaction is not stable when the measurements were repeated several times because they could be other reactions taking place. Similar results were observed in the interaction of molecular I_2 with other amines which are included in the Supporting Information (Figure S17-S19).

The interaction of I_2 with PTZ in dichloromethane resulted in the formation a new band in the UV-Visible spectrum at 450 nm (left and center). This new band suggests the formation of a complex. In addition to the new band at 450 nm, there is also a new band observed at over 500 nm which

indicates the formation of cation radical. This band indicates the presence of a cation radical, which is formed through a redox process. The appearance of this band suggests that the reaction between I_2 and PTZ involves a change in the oxidation state of one or both of the reactants. In this case, the appearance of two new bands suggests the formation of a complex and a redox process involving the transfer of an electron.

While for the interactions of I_2 with the heterocyclic compound (PTZ) in acetonitrile led to the formation of cation radical at wavelengths ranging from 500 -800 nm as shown in the Figure 5-3 (right).

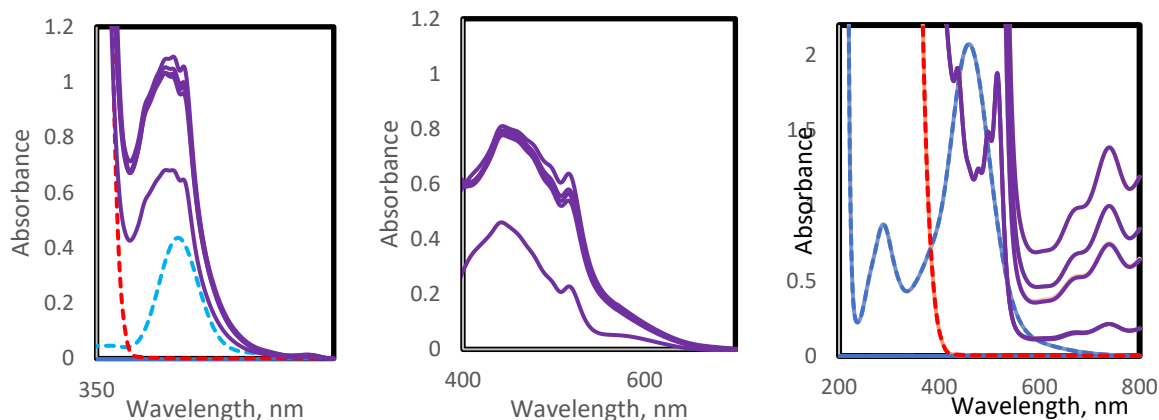


Figure 5-3. (Left) Spectra of solutions with constant I_2 concentrations and various PTZ concentrations in DCM. The spectra of the solutions of the individual reactants are shown as dashed blue (I_2) and red (PTZ) lines. (Center) Spectra of the complexes obtained by subtracting the absorption of components from the spectra of their mixtures in DCM. (Right) Spectra of the solutions with constant concentrations of I_2 and various concentrations of PTZ in AN.

The addition of I_2 electrophiles to MPTZ solutions in dichloromethane resulted in a new absorption band at ~ 480 nm, which was not present in the spectra of the separate components. This band was persistent, and its intensity increased with increasing amine concentration at a constant concentration of I_2 and was slightly red-shifted as shown in Figure S20 in the Supporting Information.

The interaction of I₂ with MPTZ in acetonitrile also led to the formation of cation radical with wavelength at about 500-800 nm which suggest redox process. The values of the experimental UV-Vis spectra were fitted to Equation 24 (Experimental Section), which describes the changes in these characteristics with the addition of nucleophiles to the solutions of halogenated molecules. This fitting was performed using Origin 2016. In the fitting procedure, UV-Vis absorption intensities were plotted against increasing amine concentrations with a constant concentration of iodine molecules, and the formation constants of the halogen-bonded complexes were generated. The values of the formation constants and coefficient of absorptivity is shown in the Table 5-1 below and an example of such a fitting is shown in Figure 5-4, while that of other aromatic amine are shown in Figure S21 in the Supporting Information.

Table 5-1. Formation constants and coefficients of absorptivity of halogen bonded complexes

Amines	$K_{\text{HaB}}, \text{M}^{-1}$	$\epsilon, \text{M}^{-1}\text{cm}^{-1}$
DMACN	2.0±0.3	201±27
DMABr	7.1±0.3	970±25
DMAF	25.8±0.5	629±4
pMeODMA	150.0±7.0	998±38
MPTZ	7.0±1.03	253±24

It is important to note that the formation constant of the complex formed when I₂ interacted with DABCO has been determined over 50 years and it's said to be very high which is $\sim 10^5 \text{M}^{-1}$. While the interaction of I₂ and TMPD is very fast and produced cation radical.

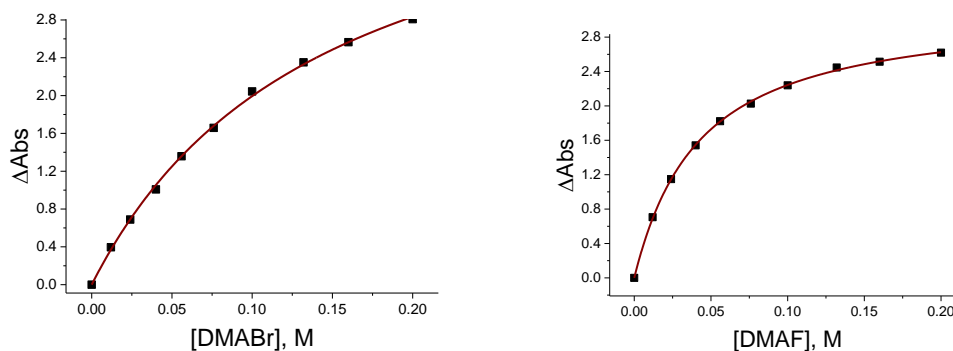


Figure 5-4. Dependencies of the ΔAbs and $\Delta\delta$ values in the solutions with a constant concentration of I_2 and variable aliphatic and aromatic amine concentrations.

5.3 Computational Data

The DFT calculations performed to optimize the complexes and the interaction energies was calculated with equation: $\Delta E = E_{comp} - (E_{I_2} + E_{Amines}) + BSSE$, as shown in the Table 5-2 below.

Table 5-2: Energies of HaB complexes between I_2 and amines obtained from M06-2X/def-TZVPP computations (in vacuum, dichloromethane, and acetonitrile) using PCM model.

Amines	ΔE , kcal/mol		
	DCM	AN	Vacuum
DMA	-8.1	-8.3	-7.7
DMABr	-7.2	-7.3	-7.0
DMACN	-4.9	-4.9	-5.2
DMAF	-8.3	-8.5	-7.9
p-MeODMA	-9.6	-10.0	-9.1
m-MeODMA	-8.0	-8.1	-8.0
TMPD	-11.0	-11.0	-10.8
MPTZ	-6.7	-7.4	-7.2
PTZ	-7.1	-5.6	-6.4
Thiantrene	-5.3	-5.3	-5.2

The energies of the HaB of I₂ with amines in different media such as vacuum, DCM and AN, and the energies of the individual molecules and their ZPE values in hartrees are shown in Table S5 in the Supporting Information. From the table above, the computed energies for the I₂-amine complexes were relatively close. Overall, the results in the table 5.2 suggest that the strength of the halogen bonding interactions in the I₂-amine complexes does not depend significantly on the media or environment.

The electron transfer reactions between I₂ (molecular iodine) and amines can exhibit two different reaction mechanisms, leading to the formation of different products. These mechanisms are known as electron transfer final (ETF) and electron transfer (ET).

In the ETF mechanism, the reaction involves 3/2I₂ (three halves of iodine) and an amine molecule (A). During the reaction, one amine molecule transfers an electron to 3/2I₂, resulting in the formation of I₃⁻ (triiodide anion) and A⁺ (Amine cation radical). This process can be represented by the equation:



On the other hand, in the ET mechanism, the reaction involves one molecule of I₂ and an amine molecule (A). In this case, the amine molecule transfers an electron to I₂, generating I₂⁻ (diiodide anion) and A⁺ (Amine cation radical). The equation representing this process is:



Both reaction mechanisms involve electron transfer between the iodine species and the amine molecule, resulting in the formation of diiodide anions (I₂⁻) or triiodide (I₃⁻) and amine cation radical (A⁺). The specific mechanism that occurs in a given reaction depends on the stoichiometry of the reactants.

It's important to note that the stoichiometric coefficients (3/2 in Equation 1) indicate the ratio of reactants required to achieve a balanced reaction. This fractional coefficient arises because the reaction involves multiple iodine molecules to transfer a specific number of electrons. The actual reaction conditions and concentrations would determine the appropriate ratio of reactants in practice. The difference in the energies obtained were calculated based on these two mechanisms proposed for the electron transfer reaction. The energetics for the mechanism proposed first were computed using the equation: $\Delta E = (E_{A^+} + E_{I_3^-}) - (E_A + 1.5E_{I_2})$ for electron transfer final (ETF). The energetics for the mechanism proposed second were computed using the equation: $\Delta E = (E_{A^+} + E_{I_2^-}) - (E_A + E_{I_2})$, and it is shown in Table 5-3.

Table 5-3: Energies ET reactions of HaB complexes between I₂ and amines resulting from M06-2X/def-TZVPP computations (vacuum, dichloromethane, and acetonitrile) using the PCM model.

Amines ET Reaction	$\Delta E(ETF)$, kcal/mol			$\Delta E(ET)$, kcal/mol		
	DCM	AN	Vacuum	DCM	AN	Vacuum
DMA	7.2	0.3	82.2	23.8	16.2	105.7
DMABr	9.0	1.9	83.3	25.6	17.8	106.8
DMACN	17.2	9.6	94.9	33.9	25.5	118.4
DMAF	6.7	-0.5	82.5	23.3	15.4	105.9
p-MeODMA	-1.7	-8.3	70.0	15.0	7.6	93.4
m-MeODMA	53.0	-0.6	78.5	69.6	15.3	102.0
TMPD	-13.0	-19.4	55.6	3.6	-3.5	79.1
MPTZ	3.6	-3.4	72.9	20.2	12.5	96.3
PTZ	1.0	-5.6	72.1	17.6	10.3	95.6
Thiantrene	13.9	7.4	84.4	30.5	23.3	107.9

The results show the calculated energies for electron transfer reactions (ET reactions) between I₂ and various amines. The results showed that the ΔE values varied depending on the amine and solvent used. The ΔE values were generally higher in vacuum than those in DCM or AN. This suggests that ET reactions are most favorable in acetonitrile because of the polarity of this medium, which allows for a redox reaction and is least favorable in vacuum.

5.4 Conclusion

- The HaB complexes were characterized by strong absorption bands in the UV range. HyB complexes are characterized by UV-Vis absorption, similar to the superposition of bands of the corresponding separate molecules (no new bands).
- HaB complexes were characterized by an upfield shift of the proton NMR signals of CHX₃ and (halo)imidazolium with halogen substituents.
- Hydrogen-bonded complexes with aliphatic amines showed down-field shifted proton NMR signals, but the direction of shifts with aromatic amines varied with the structure of the complexes. In contrast, the NMR signals of the hydrogen-substituted (halo)imidazolium were consistent with those of aliphatic amines.
- Simultaneous treatment of the UV-Vis and NMR titration data made it possible to evaluate the formation constants of the competing HaB and HyB complexes. The fitting of the UV-Vis titration data of the interactions of iodine with aromatic amines was performed separately, similar to that of the UV-Vis and NMR titration data involving (halo)imidazolium salts and halides, and the formation constants were computed.
- The σ -hole model explains variations in K_{HaB} and K_{HyB} , provided that the polarization of CHX₃ by Amines is considered.
- The strength of halogen bonding interactions in the I₂-amine complexes remains relatively consistent regardless of the media or environment.
- The calculated energies for electron transfer reactions (ET reactions) between I₂ and different amines indicated that the ΔE values vary depending on the solvent, with acetonitrile (AN) being the most favorable medium due to its polarity, allowing for a redox reaction, while vacuum is the least favorable.

REFERENCES

1. Freedman, H. H., Intramolecular H-bonds. I. A spectroscopic study of the hydrogen bond between hydroxyl and nitrogen. *Journal of the American Chemical Society* **1961**, *83* (13), 2900-2905.
2. Steiner, T., The hydrogen bond in the solid state. *Angewandte Chemie International Edition* **2002**, *41* (1), 48-76.
3. Benjamin, S. L.; Levason, W.; Pugh, D.; Reid, G.; Zhang, W., Preparation and structures of coordination complexes of the very hard Lewis acids ZrF₄ and HfF₄. *Dalton Transactions* **2012**, *41* (40), 12548-12557.
4. Solovyev, A.; Chu, Q.; Geib, S. J.; Fensterbank, L.; Malacria, M.; Lacote, E.; Curran, D. P., Substitution Reactions at Tetracoordinate Boron: Synthesis of N-Heterocyclic Carbene Boranes with Boron– Heteroatom Bonds. *Journal of the American Chemical Society* **2010**, *132* (42), 15072-15080.
5. Cavallo, G.; Metrangolo, P.; Milani, R.; Pilati, T.; Priimagi, A.; Resnati, G.; Terraneo, G., The Halogen Bond. *Chem Rev* **2016**, *116* (4), 2478-601.
6. Stromme, K., An X-Ray Analysis of the 1: 1 Compound Trimethylamine-Iodine. *Acta Chem. Scand* **1959**, *13* (2).
7. Rissanen, K., Halogen bonded supramolecular complexes and networks. *CrystEngComm* **2008**, *10* (9), 1107-1113.
8. Chandran, S. K.; Thakuria, R.; Nangia, A., Silver (I) complexes of N-4-halophenyl-N'-4-pyridyl ureas. Isostructurality, urea··· nitrate hydrogen bonding, and Ag··· halogen interaction. *CrystEngComm* **2008**, *10* (12), 1891-1898.

9. Metrangolo, P.; Pilati, T.; Terraneo, G.; Biella, S.; Resnati, G., Anion coordination and anion-templated assembly under halogen bonding control. *CrystEngComm* **2009**, *11* (7), 1187-1196.
10. Schulz, N.; Sokkar, P.; Engelage, E.; Schindler, S.; Erdelyi, M.; Sanchez-Garcia, E.; Huber, S. M., The interaction modes of haloimidazolium salts in solution. *Chemistry–A European Journal* **2018**, *24* (14), 3464-3473.
11. Gilday, L. C.; Robinson, S. W.; Barendt, T. A.; Langton, M. J.; Mullaney, B. R.; Beer, P. D., Halogen Bonding in Supramolecular Chemistry. *Chem Rev* **2015**, *115* (15), 7118-95.
12. Loy, C.; Holthoff, J. M.; Weiss, R.; Huber, S. M.; Rosokha, S. V., "Anti-electrostatic" halogen bonding in solution. *Chem Sci* **2021**, *12* (23), 8246-8251.
13. Decato, D. A.; John, E. A.; Berryman, O. B., Halogen Bonding: An Introduction. In *Halogen Bonding in Solution*, 2021; pp 1-41.
14. Clark, T.; Hennemann, M.; Murray, J. S.; Politzer, P., Halogen bonding: the σ -hole. *Journal of molecular modeling* **2007**, *13* (2), 291-296.
15. Murray, J. S.; Macaveiu, L.; Politzer, P., Factors affecting the strengths of σ -hole electrostatic potentials. *Journal of Computational Science* **2014**, *5* (4), 590-596.
16. Awwadi, F. F.; Willett, R. D.; Peterson, K. A.; Twamley, B., The nature of halogen... halogen synthons: Crystallographic and theoretical studies. *Chemistry–A European Journal* **2006**, *12* (35), 8952-8960.
17. Lieffrig, J.; Jeannin, O.; Frąckowiak, A.; Olejniczak, I.; Świetlik, R.; Dahaoui, S.; Aubert, E.; Espinosa, E.; Auban-Senzier, P.; Fourmigué, M., Charge-assisted halogen bonding: donor–acceptor complexes with variable ionicity. *Chemistry–A European Journal* **2013**, *19* (44), 14804-14813.

18. Wang, P.; Zhao, N.; Tang, Y., Halogen Bonding in the Complexes of CH₃I and CCl₄ with Oxygen-Containing Halogen-Bond Acceptors. *J Phys Chem A* **2017**, *121* (26), 5045-5055.
19. Fourmigué, M.; Lieffrig, J., Organizing radical species in the solid state with halogen bonding. *Halogen Bonding II: Impact on Materials Chemistry and Life Sciences* **2015**, 91-113.
20. Atzori, M.; Serpe, A.; Deplano, P.; Schlueter, J. A.; Mercuri, M. L., Tailoring magnetic properties of molecular materials through non-covalent interactions. *Inorganic Chemistry Frontiers* **2015**, *2* (2), 108-115.
21. Oswald, I. D.; Allan, D. R.; Motherwell, W. S.; Parsons, S., Structures of the monofluoro- and monochlorophenols at low temperature and high pressure. *Acta Crystallographica Section B: Structural Science* **2005**, *61* (1), 69-79.
22. Metrangolo, P.; Resnati, G., *Halogen bonding: fundamentals and applications*. Springer: 2008; Vol. 126.
23. Auffinger, P.; Hays, F. A.; Westhof, E.; Ho, P. S., Halogen bonds in biological molecules. *Proceedings of the National Academy of Sciences* **2004**, *101* (48), 16789-16794.
24. Wilcken, R.; Zimmermann, M. O.; Lange, A.; Joerger, A. C.; Boeckler, F. M., Principles and applications of halogen bonding in medicinal chemistry and chemical biology. *J Med Chem* **2013**, *56* (4), 1363-88.
25. Chudzinski, M. G.; Taylor, M. S., Correlations between computation and experimental thermodynamics of halogen bonding. *The Journal of Organic Chemistry* **2012**, *77* (7), 3483-3491.
26. Riley, K. E.; Hobza, P., The relative roles of electrostatics and dispersion in the stabilization of halogen bonds. *Physical Chemistry Chemical Physics* **2013**, *15* (41), 17742-17751.

27. Gilday, L. C.; Robinson, S. W.; Barendt, T. A.; Langton, M. J.; Mullaney, B. R.; Beer, P. D., Halogen bonding in supramolecular chemistry. *Chemical reviews* **2015**, *115* (15), 7118-7195.
28. Trung, N. T.; Hue, T. T.; Nguyen, M. T., Interaction of CHX₃ (X= F, Cl, Br) with HNO induces remarkable blue shifts of both C–H and N–H bonds. *Physical Chemistry Chemical Physics* **2009**, *11* (6), 926-933.
29. Zhao, X. r.; Pang, X.; Yan, X. q.; Jin, W. j., Halogen bonding or hydrogen bonding between 2, 2, 6, 6-tetramethylpiperidine-oxyl radical and trihalomethanes CHX₃ (X= Cl, Br, I). *Chinese Journal of Chemical Physics* **2013**, *26* (2), 172.
30. Rosokha, S. V.; Neretin, I. S.; Rosokha, T. Y.; Hecht, J.; Kochi, J. K., Charge-transfer character of halogen bonding: Molecular structures and electronic spectroscopy of carbon tetrabromide and bromoform complexes with organic σ - and π -donors. *Heteroatom Chemistry* **2006**, *17* (5), 449-459.
31. Bertolotti, F.; Gervasio, G., Crystal structure of iodoform at 106 K and of the adduct CHI₃·3 (C₉H₇N). Iodoform as a building block of co-crystals. *Journal of Molecular Structure* **2013**, *1036*, 305-310.
32. Nayak, S. K.; Terraneo, G.; Piacevoli, Q.; Bertolotti, F.; Scilabra, P.; Brown, J. T.; Rosokha, S. V.; Resnati, G., Molecular Bases for Anesthetic Agents: Halothane as a Halogen- and Hydrogen-Bond Donor. *Angew Chem Int Ed Engl* **2019**, *58* (36), 12456-12459.
33. Green, R.; Martin, J. S., Anion-molecule complexes in solution. I. Nuclear magnetic resonance and infrared studies of halide ion-trihalomethane association. *Journal of the American Chemical Society* **1968**, *90* (14), 3659-3668.

34. Bertrán, J. F.; Rodríguez, M., Detection of halogen bond formation by correlation of proton solvent shifts. II—methylene halides in n-electron donor solvents. *Organic Magnetic Resonance* **1980**, *14* (4), 244-246.
35. Watson, B.; Grounds, O.; Borley, W.; Rosokha, S. V., Resolving the halogen vs. hydrogen bonding dichotomy in solutions: intermolecular complexes of trihalomethanes with halide and pseudohalide anions. *Phys Chem Chem Phys* **2018**, *20* (34), 21999-22007.
36. Rosokha, S. V.; Kochi, J. K., Fresh look at electron-transfer mechanisms via the donor/acceptor bindings in the critical encounter complex. *Accounts of chemical research* **2008**, *41* (5), 641-653.
37. Atkins, P.; Atkins, P. W.; de Paula, J., *Atkins' physical chemistry*. Oxford university press: 2014.
38. Rosokha, S. V., Electron-transfer reactions of halogenated electrophiles: a different look into the nature of halogen bonding. *Faraday Discussions* **2017**, *203*, 315-332.
39. Brunschwig, B. S.; Sutin, N., Energy surfaces, reorganization energies, and coupling elements in electron transfer. *Coordination chemistry reviews* **1999**, *187* (1), 233-254.
40. Rosokha, S. V.; Vinakos, M. K., Halogen bond-assisted electron transfer reactions of aliphatic bromosubstituted electrophiles. *Phys Chem Chem Phys* **2014**, *16* (5), 1809-13.
41. Rosokha, S. V.; Traversa, A., From charge transfer to electron transfer in halogen-bonded complexes of electrophilic bromocarbons with halide anions. *Physical Chemistry Chemical Physics* **2015**, *17* (7), 4989-4999.
42. Rosokha, S.; Neretin, I.; Rosokha, T.; Hecht, J.; Kochi, J., Charge-transfer character of halogen bonding: Molecular structures and electronic spectroscopy of carbon tetrabromide and

bromoform complexes with organic σ -and π -donors. *Heteroatom Chemistry: An International Journal of Main Group Elements* **2006**, 17 (5), 449-459.

PUBLICATION

Part of our work was the basis for the published article:

- 1. Adeniyi, E.;** Grounds, O.; Stephens, Z.; Zeller, M.; Rosokha, S. V., Thermodynamics and Spectroscopy of Halogen-and Hydrogen-Bonded Complexes of Haloforms with Aromatic and Aliphatic Amines. *Molecules* **2022**, 27 (18), 6124.